



# Identification of sources of coarse mode aerosol particles (PM<sub>10</sub>) using ATR-FTIR and SEM-EDX spectroscopy over the Himalayan Region of India

Sakshi Gupta<sup>1,2</sup> · Shobhna Shankar<sup>3</sup> · Jagdish Chandra Kuniyal<sup>4</sup> · Priyanka Srivastava<sup>5</sup> · Renu Lata<sup>6</sup> · Sheetal Chaudhary<sup>4</sup> · Isha Thakur<sup>6</sup> · Archana Bawari<sup>4</sup> · Shilpa Thakur<sup>6</sup> · Monami Dutta<sup>7</sup> · Abhinandan Ghosh<sup>8</sup> · Manish Naja<sup>5</sup> · Abhijit Chatterjee<sup>7</sup> · Ranu Gadi<sup>3</sup> · Nikki Choudhary<sup>1,2</sup> · Akansha Rai<sup>1,2</sup> · Sudhir Kumar Sharma<sup>1,2</sup>

Received: 15 July 2023 / Accepted: 7 January 2024 / Published online: 2 February 2024  
© The Author(s), under exclusive licence to Springer-Verlag GmbH Germany, part of Springer Nature 2024

## Abstract

This study attempts to examine the morphological, elemental and physical characteristics of PM<sub>10</sub> over the Indian Himalayan Region (IHR) using FTIR and scanning electron microscopy-energy dispersive X-ray (SEM-EDX) analysis. The study aimed at source identification of PM<sub>10</sub> by exploring the inorganic ions, organic functional groups, morphology and elemental characteristics. The pollution load of PM<sub>10</sub> was estimated as  $63 \pm 22 \mu\text{g m}^{-3}$ ;  $53 \pm 16 \mu\text{g m}^{-3}$ ;  $67 \pm 26 \mu\text{g m}^{-3}$  and  $55 \pm 11 \mu\text{g m}^{-3}$  over Mohal-Kullu, Almora, Nainital and Darjeeling, respectively. ATR-FTIR spectrum analysis revealed the existence of inorganic ions ( $\text{SiO}_4^{4-}$ ,  $\text{TiO}_2$ ,  $\text{SO}_4^{2-}$ ,  $\text{SO}_3^-$ ,  $\text{NO}_3^-$ ,  $\text{NO}_2^-$ ,  $\text{CO}_3^{2-}$ ,  $\text{HCO}_3^-$ ,  $\text{NH}_4^+$ ) and organic functional groups (C–C, C–H, C=C, C≡C, C=O, N–H, C≡N, C=N, O–H, cyclic rings, aromatic compounds and some heterogeneous groups) in PM<sub>10</sub> which may arise from geogenic, biogenic and anthropogenic sources. The morphological and elemental characterization was performed by SEM-EDX, inferring for geogenic origin (Al, Na, K, Ca, Mg and Fe) due to the presence of different morphologies (irregular, spherical, cluster, sheet-like solid deposition and columnar). In contrast, particles having biogenic and anthropogenic origins (K, S and Ba) have primarily spherical with few irregular particles at all the study sites. Also, the statistical analysis ANOVA depicts that among all the detected elements, Na, Al, Si, S and K are site-specific in nature as their mean of aw% significantly varied for all the sites. The trajectory analysis revealed that the Uttarakhand, Jammu and Kashmir, the Thar Desert, Himachal Pradesh, Pakistan, Afghanistan, Nepal, Sikkim, the Indo-Gangetic Plain (IGP) and the Bay of Bengal (BoB) contribute to the increased loading of atmospheric pollutants in various locations within the IHR.

**Keywords** PM<sub>10</sub> · ATR-FTIR · SEM-EDX · Morphology · Elements · Organic functional groups

## Abbreviations

IHR Indian Himalayan Region  
PM Particulate matter

ATR- FTIR Attenuated total reflectance-Fourier transform infrared spectrophotometer  
SEM-EDX Scanning electron microscopy-energy dispersive X-ray  
aw% Atomic weight percentage

Responsible Editor: Gerhard Lammel

✉ Sudhir Kumar Sharma  
sudhir.npl@nic.in; sudhircsir@gmail.com

<sup>1</sup> CSIR-National Physical Laboratory, Dr. K. S. Krishnan Road, New Delhi 110012, India

<sup>2</sup> Academy of Scientific and Innovative Research (AcSIR), Ghaziabad 201002, India

<sup>3</sup> Indira Gandhi Delhi Technical University for Women, Kashmere Gate, New Delhi 110006, India

<sup>4</sup> G. B. Pant National Institute of Himalayan Environment, Kosi-Katarmal, Almora 263643, India

<sup>5</sup> Aryabhata Research Institute of Observational Sciences (ARIES), Nainital, Uttarakhand 263002, India

<sup>6</sup> G. B. Pant National Institute of Himalayan Environment, Himachal Regional Centre, Mohal-Kullu 175126, India

<sup>7</sup> Environmental Sciences Section, Bose Institute, EN Block, Sector-V, Saltlake, Kolkata 700091, India

<sup>8</sup> Department of Civil Engineering, Centre of Environmental Science and Engineering, IIT-Kanpur, Kanpur 201086, India

ANOVA	Analysis of variance
WHO	World Health Organisation
IGP	Indo-Gangetic plain
NIHE	National Institute of Himalayan Environment
ARIES	Aryabhata Research Institute of Observational Sciences
NAAQs	National Ambient Air Quality Standards
RDS	Respirable dust sampler
BoB	Bay of Bengal
PAHs	Polycyclic aromatic hydrocarbons
VOCs	Volatile organic compounds
NMVOCs	Non-methyl volatile organic compounds
SVOCs	Secondary volatile organic compounds
SOA	Secondary organic aerosols
CNN	Cloud condensation nuclei

## Introduction

The atmosphere is a dynamic natural gas system for maintaining life, and several biogenic and anthropogenic activities release pollutants into the air in one manner or another (Singh 2019). An essential aspect of the earth's atmosphere, aerosols that pass through the air are made up of a variety of particles with diverse chemical compositions, sizes (0.001 to 100  $\mu\text{m}$ ), shapes and optical properties (Ram and Sarin 2012). These are primarily confined to the lower troposphere, where there is substantial vertical and horizontal mixing. As a result, pollutants can spread and disperse over larger distances, having an impact on a wider region rather than being limited to a localized area. The transport, distribution and dispersion of pollutants in the atmosphere, which affects air quality patterns and the spatial range of pollution impacts, are all influenced by this vertical and horizontal mixing (Ram and Sarin 2012). High levels of aerosols and poor air quality have a negative impact on the environment and human health in urban areas (Belis et al. 2013; Jerrett 2015; Lelieveld et al. 2015). It causes unfavourable climatic conditions, respiratory issues, cardiovascular diseases and altered atmospheric chemistry, highlighting the urgent need for emission controls, the adoption of renewable energy sources, sustainable transportation and international cooperation to lessen the negative effects of air pollution (Cheng et al. 2007; Pope et al. 2009; Bond et al. 2013; Panwar et al. 2020; Joshi et al. 2022). Several regions worldwide observe that the concentrations of the pollutants exceed the ambient air quality standards laid by World Health Organization (WHO) (Arun et al. 2021; Bharti et al. 2017; Jain et al. 2020; Shankar et al. 2022; Shankar et al. 2023b). The chemical constituents of aerosols also change spatially and temporally, which affects air quality (Jerrett 2015; Lelieveld et al. 2015), visibility, Earth's radiation budget, global climate (Ramanathan et al. 2001) and human health

(Colonna et al. 2022; Dockery et al. 1993; Joshi et al. 2022; Pope and Dockery 2006).

Air pollution has a significant impact on the ecosystem, climate, monsoon, water, agriculture and human wellness in the IHR (Kuniyal and Guleria 2010; Guleria et al. 2012; Adak et al. 2014; Sharma et al. 2020a, 2020b; Chatterjee et al. 2021; Choudhary et al. 2022). The problem of air pollution is becoming more severe in the IHR, and majority of the pollution is brought in from the Indo-Gangetic plains (IGP) (Choudhary et al. 2022; Jain et al. 2019; Sharma et al. 2020a, 2020b) and surrounding regions. Environmental elements, including air, water, soil, land and forest, in the Himalayas have decreased due to increased tourism in the region (Davies and Cahill 2000). Overcrowding of residents and visitors in a particular hill station is one of the leading causes of air pollution (Chatterjee et al. 2021; Choudhary et al. 2022). Most of the IHR's hill stations have been turned into cities, which are gradually being populated by people moving there from all over India and overseas (Singh 2019). The problems with air pollution experienced by hill towns in IHR include burning of biomass, excessive fossil fuel consumption, forest fires and vehicular emissions brought on by an overabundance of tourists. The climate of IHR is negatively impacted by unauthorized planning (at the policy level), pollutant movement from the IGP, deforestation and ignorance of the health implications of air pollution (Cheng et al. 2009; Choudhary et al. 2023; Sharma et al. 2020a, 2020b). The health effects of particulate matter (PM) are influenced by several factors, including exposure dose, chemical composition, morphological properties, surface reactivity, hydrophobicity, hydrophilicity and solubility following deposition in the target site. Recent studies (Rai et al. 2021; Sharma et al. 2021; Choudhary et al. 2022, 2023) demonstrated the abundance of carbonaceous components, water-soluble inorganic species and elements in the  $\text{PM}_{10}$  and their potential sources over the IHR.

A number of studies have been conducted in recent years on carbonaceous, inorganic and elemental species in PM and their sources in urban (Gupta et al. 2018; Jain et al. 2020, 2021; Mandal et al. 2014; Ram and Sarin 2011; Sharma et al. 2016; Shivani et al. 2019), rural (Begam et al. 2017) as well as high-altitude atmosphere (Ram et al. 2008; Kumar and Attri 2016; Sarkar et al. 2017a; Kaushal et al. 2018; Sharma et al. 2020a, 2020b; Rai et al. 2021; Choudhary et al. 2022), but limited study has been conducted in the identification of sources of PM using attenuated total reflectance-Fourier transform infrared spectrophotometry (ATR-FTIR) and scanning electron microscopy-energy dispersive X-ray (SEM-EDX) spectroscopy in India and other polluted regions (Bharti et al. 2017; Karaca et al. 2019; Neupane et al. 2020; Sreejith et al. 2020; Pongpiachan et al. 2022; Kumar and Jain 2022; Shankar et al. 2022; Shankar et al. 2023a, b; Kimothi et al. 2023). In the present study, we applied the ATR-FTIR to identify the

likely sources of PM<sub>10</sub> through their functional groups. This approach enables a quick and qualitative analysis of a sample by identifying discrete intensity peaks associated with specific chemical bonds and functional groups. One of the key advantages of FTIR is that it eliminates the need for prior sample preparation, making the analysis process faster. Additionally, FTIR requires only a small sample size (~ 2 mm) and is non-destructive, preserving the integrity of the sample for further analysis. Scanning electron microscopy (SEM) is employed to visualize and analyse the morphology, size and shape of particles at high magnification, simultaneously with energy-dispersive X-ray spectroscopy (EDX) which is utilized to obtain qualitative and semi-quantitative elemental analysis. EDX provides information about the atomic weight percentage (aw%) of identified elements within a given particle or sample, allowing us to assess the relative proportions of specific elements in relation to other elements present. Together, SEM-EDX analysis offers valuable insights into the morphology and elemental composition of PM<sub>10</sub> samples over the IHR (western Himalayas: Mohal-Kullu, central Himalayas: Almora and Nainital and eastern Himalayas: Darjeeling). Through this comprehensive analysis, we gain a better understanding of the sources and characteristics of PM present in these areas. Overall, this research advances our knowledge of air pollution in the Himalayas and assists policymakers, lawmakers and scientists in their efforts to safeguard the region's air quality and promote sustainable development.

## Material and methods

### Study area

The study areas were selected to represent the stretch of the IHR, which spans from the western, central, to eastern Himalayan ranges (Fig. 1). The brief site description is given below:

**Western Himalayas** Western Himalayas stretched from Afghanistan to North India (Jammu & Kashmir, Ladakh and Himachal Pradesh). This area experienced the lowest rainfall (annual average, 259 mm) among IHR and received maximum precipitation in the post-monsoon season (429 mm). PM<sub>10</sub> samples were collected at G.B. Pant National Institute of Himalayan Environment (NIHE), Himachal Regional Centre, Mohal-Kullu (31.9°N, 77.11°E, 1154 m above mean sea level (amsl)). The transboundary movement of air masses is significantly influenced by nearby activities (such as biomass burning for household heating, forest fires for the growth of delicate grass for grazing of livestock population in following year and local meteorology), as well as increased automotive emissions (Choudhary et al. 2022; Guleria et al. 2012; Kuniyal and Guleria 2010).

**Central Himalayas** This part of IHR attains maximum height as it lies in the Siwalik range of the Great Himalayas. Temperature is highest in summer monsoon (25 °C) and lowest in winter (3 °C). This region receives maximum rainfall (558 mm) in summer. The G.B. Pant National Institute of Himalayan Environment (NIHE) from Kosi-Katarmal, Almora (29.59°N, 79.65°E, 1225 m amsl) and Aryabhata Research Institute of Observational Sciences (ARIES) situated in Manora Hills of Nainital (29.39°N, 79.45°E, 1959 m amsl) were selected for PM<sub>10</sub> sampling (Choudhary et al. 2022).

**Eastern Himalayas** Eastern Himalayas extended from Eastern Nepal across North-East India, Bhutan, China and Northern Myanmar. This area receives maximum rainfall (annual average, 3092 mm) among IHR and the highest precipitation in south-east monsoon in summer. This region generally has higher temperatures and precipitation than the western Himalayas. The Bose Institute from Darjeeling (27.01°N, 88.15°E, 2200 m amsl) was chosen for the sampling site. Geographically, Darjeeling is close to the IGP region, which is known for having high aerosol loadings and is heavily influenced by tourism and biomass burning (Adak et al. 2014; Chatterjee et al. 2021; Choudhary et al. 2022). The detailed description/characteristics of the study sites are available in previous publications (Choudhary et al. 2022; Guleria et al. 2012; Kuniyal and Guleria 2010; Rai et al. 2020; Sharma et al. 2020a, 2020b; Sheoran et al. 2021).

**Sampling of PM<sub>10</sub>** To study the mass concentration of PM<sub>10</sub>, the samples were collected on a pre-combusted (550 °C) Pall-flex quartz fibre filter using a high-volume respirable dust sampler (Model: APM 460 NL, M/s. Envirotech, Delhi, India) at four semi-urban locations (NIHE, Himachal Regional Centre, Mohal-Kullu ( $n = 55$ ); NIHE, Kosi-Katarmal, Almora ( $n = 105$ ); ARIES, Nainital ( $n = 63$ ) and Bose Institute, Darjeeling ( $n = 95$ )) from January to December, 2019. The average flow rate of the sampler was 1.2 m<sup>3</sup> min<sup>-1</sup> with a flow accuracy of  $\pm 2\%$  of full scale. Following the standard operating procedure, 24-h sampling of PM<sub>10</sub> was carried out in all the study sites. Before and after sampling, filters were desiccated, and initial and final weights were calculated using a microbalance having a resolution of  $\pm 10 \mu\text{g}$ . The concentration of PM<sub>10</sub> was quantified gravimetrically. Detailed sampling procedures and instrumentation are available in previous publications (Choudhary et al. 2022).

### Measurements

#### ATR-FTIR

An FTIR spectrometer (Model: SHIMADZU FTIR IRAffinity-1S) performs a qualitative analysis of inorganic ions and organic functional groups and their bond information in PM<sub>10</sub> samples. The equipment was used to gather the spectral data

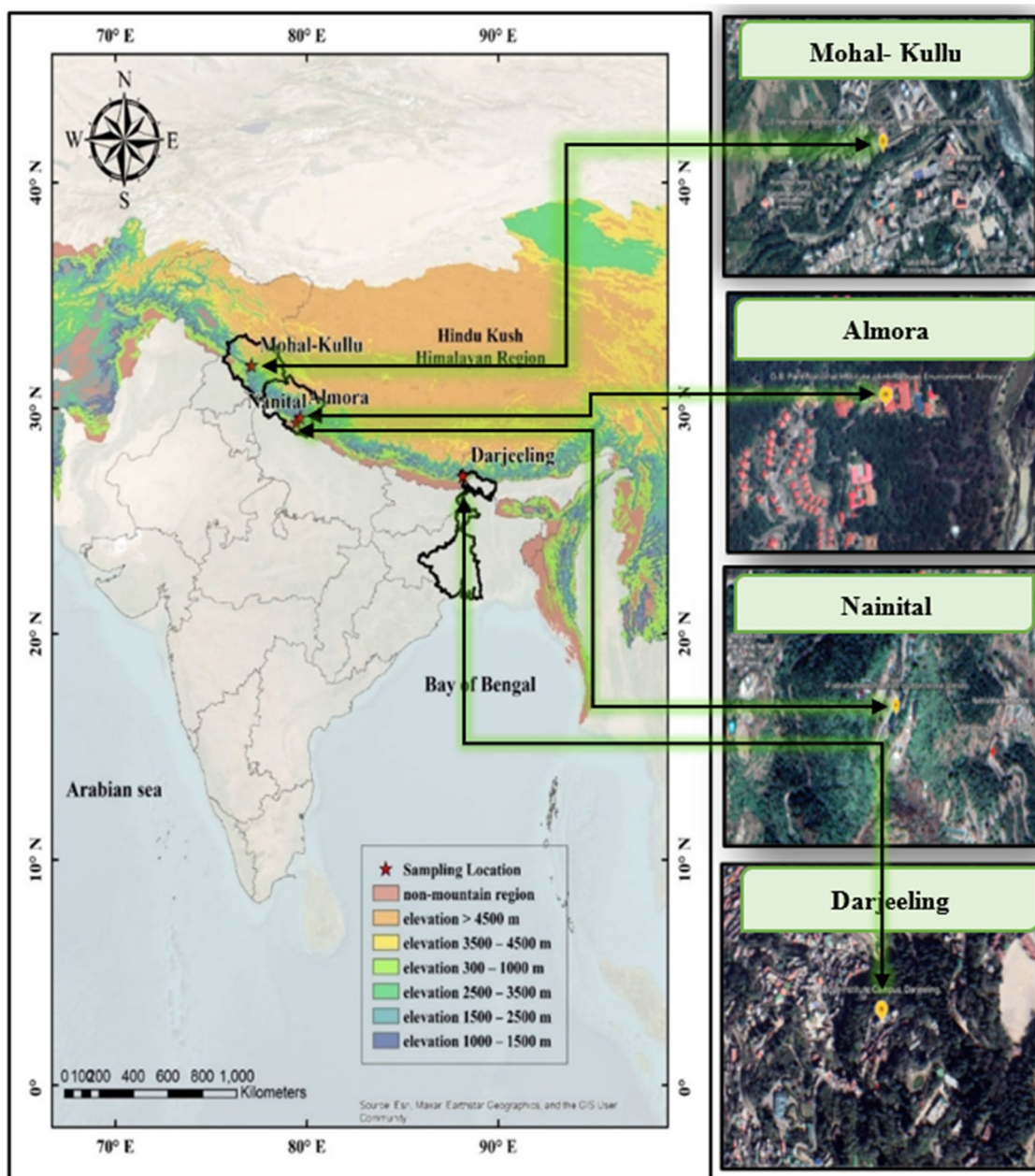


**Fig. 1** Different sampling locations in the IHR

and an ATR (QUEST ATR) accessory (diamond crystal) using Lab Solutions IR software. In order to expose the ATR crystal directly to the IR radiation, a small circular portion of the loaded sample filter with a diameter of approximately 2 mm was inverted over it. Firstly, the background spectrum of the ATR crystal was measured and then removed from the sample spectrum before measuring the FTIR spectra of the sample. The IR spectra were collected across a range of 4000–400  $\text{cm}^{-1}$  wave numbers at a resolution of 4  $\text{cm}^{-1}$  using 80 scans. Since absorption is proportional to concentration, the final spectrum was produced by subtraction of the loaded from the unloaded

spectrum of the filter. Before each scan, the ATR crystal was washed with ethanol and solely dried to remove contamination; avoiding this step could result in the –OH groups showing multiple peaks, which would be misleading (Neupane et al. 2020; Shankar et al. 2022; Shankar et al. 2023b).

**SEM-EDX**

NeoScope software was used to analyse the morphology and elemental composition ( $Z > 11$ ) of individual particles



using an SEM-EDX (Model: JEOL JCM 7000) operating at a high vacuum having an accelerating voltage of 10 kV and pre-programmed counting period of 10 s per particle scan. A small section of the PM<sub>10</sub> sample deposited on the filter (~ 8 mm<sup>2</sup>) was punched out and coated with gold using a gold sputter coater before the analysis. Using the standard less ZAF correction approach (the atomic-number effect (Z), the absorption effect (A) and the fluorescence excitation (F) effect all have an impact on the intensity of the distinctive X-rays that are released), the intensities of the characteristic X-ray lines were transformed into the relevant elemental concentration. The elemental concentrations were calculated as a aw% (Shankar et al. 2023a, 2023b).

The study aimed to assess if there were significant differences in the aw% among the four sampling sites. To achieve this, an analysis of variance (ANOVA) was performed on the estimated elements. ANOVA allows for simultaneous comparison of the average aw% across multiple sites (Kumar 2017). The null hypothesis assumed that there was no significant difference between the means of the observed elements at all four locations, while the alternative hypothesis stated that there was a significant difference in the mean atomic weight of at least one study site. ANOVA analysis was conducted using Microsoft Excel (2021) as a single-factor ANOVA test.

## Identification of sources and source region

### EF and PCA

The enrichment factor (EF) for elements of PM<sub>10</sub> were computed using the procedure described in Taylor and McLennan's work from 1985, where Eq. (1) used to determine the most likely source of elemental species in PM<sub>10</sub>:

$$EF = \frac{El_{sample}/X_{sample}}{El_{crust}/X_{crust}} \quad (1)$$

where  $El_{sample}$  and  $X_{sample}$  stand for the mass concentration of the elemental ( $El$ ) and the mass concentration of the reference element ( $X$ ) in the sample, respectively. Because of its stability and extensive distribution across the Earth's crust, Al was chosen as the reference element. The terms " $El_{crust}$ " and " $X_{crust}$ " reflect the mass concentration of elementals and the abundance of reference elements, respectively, in the upper continental crust (Gupta et al. 2023; Sharma et al. 2016).

Principal component analysis (PCA) was used to determine the probable sources of different elemental species measured by EDX in PM<sub>10</sub> particles. PCA uses orthogonal decomposition to isolate discrete components, which are then loaded factors correlated with variables. The detailed information is available in Song et al. (2006) as well as Sharma and Mandal (2023).

## Air Mass Backward Trajectories and PSCF

Backward trajectory analysis of air masses was conducted utilizing the Air Resource Laboratory (ARL) datasets under the National Oceanic and Atmospheric Administration (NOAA). The Hybrid Single Particle Lagrangian Integrated Trajectory (HYSPLIT) model, accessible at <http://ready.arl.noaa.gov/HYSPLIT.php>, was employed to trace the air mass pathway of particulate matter (PM<sub>10</sub>) from the receptor site. Using the TrajStat software, 72-h backward trajectories at 500 m above ground level (AGL) for the sampling day were generated and analysed. Air masses carry a particular concentration of pollutants, as determined by the potential source contribution function (PSCF) (Anil et al. 2019; Anil and Alagha 2020; Choudhary et al. 2022; Rai et al. 2020, 2021).

### CBPF

Striving to represent the measured concentration in polar coordinates for a comprehensive understanding of the source regions, conditional bivariate probability function (CBPF) is a novel approach (Uria-Tellaetxe and Carslaw 2014). The probability function scrutinizes wind direction (WD) and wind speed (WS) intervals characterized by elevated mass concentrations, thereby providing the likelihood of the source region. In the current investigation, the Open-air package in R-studio software (<http://www.rstudio.com/>) was utilized to implement the CBPF programming. Meteorological data, including WS with an accuracy of approximately ± 2% of the full scale, and WD with an accuracy of approximately ± 3°, were gathered through automatic weather stations (AWS) at designated sampling sites throughout the study duration from 2019 onwards (Choudhary et al. 2023). Additionally, the polar plot function was employed with the statistics set to CPF, focusing on the pollutant PM<sub>10</sub>, and considering 75 percentiles for the study at hand.

## Results and discussion

### PM<sub>10</sub> concentration

The annual average concentrations of PM<sub>10</sub> in all the four observation sites Mohal-Kullu, Almora, Nainital and Darjeeling were found to be  $63 \pm 22 \mu\text{g m}^{-3}$  (range, 11–173  $\mu\text{g m}^{-3}$ ),  $53 \pm 16 \mu\text{g m}^{-3}$  (range, 15–187  $\mu\text{g m}^{-3}$ ),  $67 \pm 26 \mu\text{g m}^{-3}$  (range, 18–250  $\mu\text{g m}^{-3}$ ) and  $55 \pm 11 \mu\text{g m}^{-3}$  (range, 21–116  $\mu\text{g m}^{-3}$ ), respectively (Fig. S1, in supplementary information). The highest annual average concentration of PM<sub>10</sub> was estimated in Nainital, followed by Mohal-Kullu, Darjeeling and Almora. Among all the four study sites, the average concentration of PM<sub>10</sub> at Nainital and Mohal-Kullu exceeded the National Ambient Air Quality Standards (NAAQS) (PM<sub>10</sub> annual, 60  $\mu\text{g m}^{-3}$ ) due to local and regional pollution

sources (mainly from IGP region) and changes in land-use patterns (Choudhary et al. 2022). Therefore, the pollution load of the central Himalayas was observed to be higher than the eastern and western Himalayan regions (Sharma et al. 2020a, 2020b). Shashni et al. (2018) found that the  $PM_{10}$  concentration in the Great Himalayan National Park (Himachal Pradesh) was  $25 \pm 2 \mu\text{g m}^{-3}$ , which is half of the estimated concentration ( $63 \pm 22 \mu\text{g m}^{-3}$ ) in Mohal-Kullu (Himachal Pradesh). This difference could be attributed to several factors, including the increased tourism in Himachal Pradesh by 4.63% compared to 2018 (Himachal Tourism Statistics 2023), heightened biomass burning activities in the region. Himachal Pradesh's notable consumption of bio-fuels, with per capita daily rates of 1.31 kg for firewood, 0.14 kg for crop residue and 0.22 kg for dung cake, surpassing those of other states in India, might also play a role (Aggarwal and Chandel 2010). Additionally, the long-range transport of pollution particles from the Indo-Gangetic Plain (IGP) and surrounding regions could contribute to the observed variations (Choudhary et al. 2022, 2023).

### ATR- FTIR analysis

The characteristic FTIR spectrum of the samples for  $PM_{10}$  is shown in Fig. 2. Tables 1 and 2 are the lists of the functional

groups and bonds that have been identified as a function of wave numbers. According to the qualitative study of  $PM_{10}$ , nearly identical peaks were seen in all samples from January to December, 2019, for all four locations, suggesting similarity in structural and functional groupings. It is generally known that the quantity of chemical functional groups depends on the characteristics of the emission sources as well as weather conditions. However, the peak strength changed depending on meteorological conditions, and the presence or absence of particular sources contributed to that group.

### Inorganic functional groups

The ATR-FTIR spectra of  $PM_{10}$  samples of all four locations (Mohal-Kullu, Almora, Nainital and Darjeeling) of IHR revealed the presence of inorganic ions ( $SiO_4^{4-}$ ,  $TiO_2$ ,  $SO_4^{2-}$ ,  $SO_3^-$ ,  $NO_3^-$ ,  $NO_2^-$ ,  $CO_3^{2-}$ ,  $HCO_3^-$  and  $NH_4^+$ ) (Table 1). For sampling purposes, we acquire quartz fibre filters that have a silicate composition. Therefore, there is a sharp peak for  $SiO_4^{4-}$  at all the locations, Mohal-Kullu and Nainital ( $455\text{--}460 \text{ cm}^{-1}$ ), Almora ( $457\text{--}466 \text{ cm}^{-1}$ ) and Darjeeling ( $455\text{--}466 \text{ cm}^{-1}$ ) (Anil et al. 2014; Bharti et al. 2017; Shankar et al. 2022; Sreejith et al. 2020). Sampling sites are hilly areas; hence, various dust events contribute to the pollution source as dust and crustal minerals (Choudhary

**Fig. 2** Representative ATR-FTIR spectra (spectral range,  $400\text{--}4000 \text{ cm}^{-1}$ ) of  $PM_{10}$  over IHR

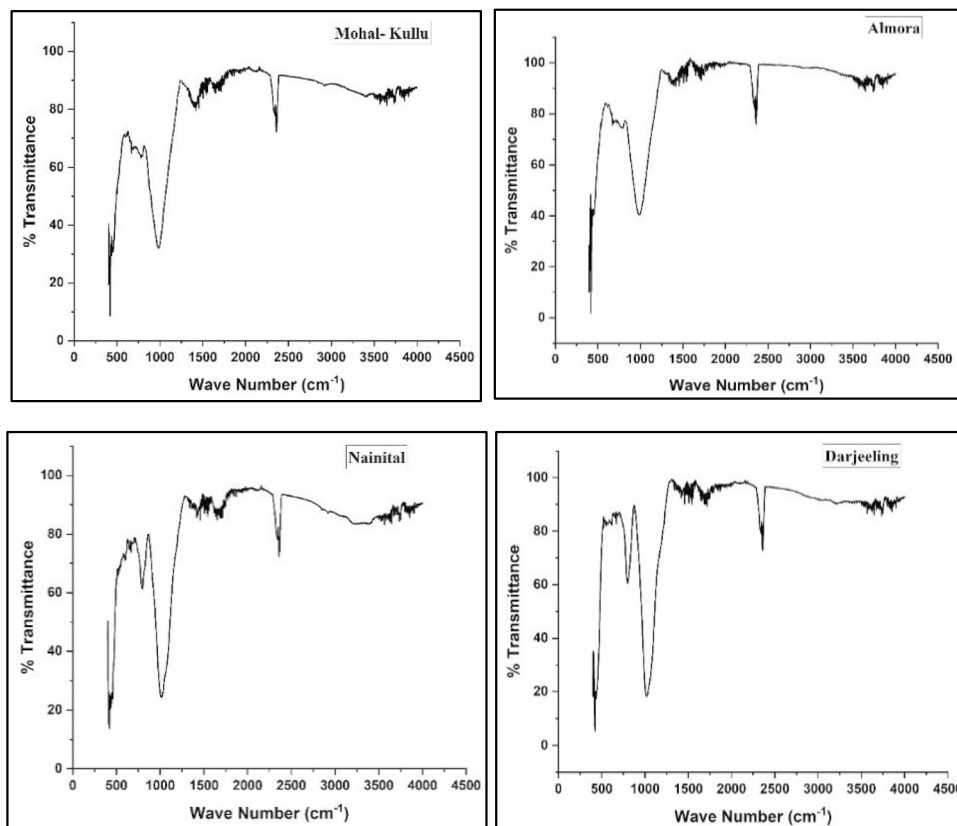


**Table 1** ATR-FTIR intensity peaks ( $\text{cm}^{-1}$ ) for inorganic ions present in  $\text{PM}_{10}$  at the study sites

Ions	Mohal-Kullu	Almora	Nainital	Darjeeling	References
$\text{SiO}_4^{4-}$	455–460	457–466; 999–1001	455–460; 999	445–466; 1002–1008	Anil et al. (2014); Bharti et al. (2017); Larkin (2018); Sreejith et al. (2020); Shankar et al. (2022)
$\text{TiO}_2$	536–541; 669	536–538; 655–669	538–545; 659–677	536–549; 655–669	Larkin (2018)
$\text{SO}_4^{2-}$	613–619	615–623	613–617	611–619	Anil et al. (2014); Bharti et al. (2017); Larkin (2018); Sreejith et al. (2020); Shankar et al. (2022); Pongpiachan et al. (2022); Kumar et al. (2023)
$\text{SO}_3^-$	975–993	977–999	–	–	Larkin (2018)
$\text{NO}_3^-$	713–727; 825–833; 1381–1404	719; 827–833; 1381–1396	713–721; 819–821; 1394–1398	717–729; 1386–1398	Stuart (2004); Anil et al. (2014); Larkin (2018); Sreejith et al. (2020); Shankar et al. (2022); Pongpiachan et al. (2022)
$\text{NO}_2^-$	825; 1267–1278	827; 1267–1278	819–821; 1274	–	Stuart (2004); Larkin (2018)
$\text{CO}_3^{2-}$	713–721; 1448–1462	704–719; 1456–1462	713–719; 1456	717–727; 875; 1456	Anil et al. (2014); Larkin (2018); Sreejith et al. (2020)
$\text{HCO}_3^-$	1323; 1651–1658	1317–1321; 1645–1658	1317–1327; 1647–1656	1317–1328; 1645–1652	Larkin (2018)
$\text{NH}_4^+$	1413–1421	1408–1419	1411–1421	1415–1421	Bharti et al. (2017); Larkin (2018); Sreejith et al. (2020); Shankar et al. (2022)

et al. 2022). Also, various studies illustrated the transport of dust aerosols from IGP, the Thar desert, the BoB and some regional countries towards IHR (Choudhary et al. 2022; Rai et al. 2021). The sharp peak for Si–O–Si bonding in silicate dust particles occurred at wave number 999–1001  $\text{cm}^{-1}$  in Almora, 999  $\text{cm}^{-1}$  in Nainital and 1002–1008  $\text{cm}^{-1}$  in Darjeeling (Shankar et al. 2022). Titanium dioxide ( $\text{TiO}_2$ ) is the tracer for soil and crustal dust. It is also used in ore mining activities (Ilmenite and Rutile) which are coming from long-range transport in Darjeeling (Jain et al. 2019; Indian Minerals Yearbook 2018; Choudhary et al. 2023). There were two IR peaks; one shoulder peak with weak intensity (536–549  $\text{cm}^{-1}$ ) and another with strong intensity (655–677  $\text{cm}^{-1}$ ) were shown for  $\text{TiO}_2$  in all the study sites (Mohal-Kullu, 536–541  $\text{cm}^{-1}$  and 669  $\text{cm}^{-1}$ ; Almora, 536–538  $\text{cm}^{-1}$  and 655–669  $\text{cm}^{-1}$ ; Nainital, 538–545  $\text{cm}^{-1}$  and 659–677  $\text{cm}^{-1}$ ; and Darjeeling, 536–549  $\text{cm}^{-1}$  and 655–669  $\text{cm}^{-1}$ ).

Secondary aerosols, such as  $(\text{NH}_4)_2\text{SO}_4$  and  $\text{NH}_4\text{NO}_3$ , are primarily made up of their gaseous predecessors,  $\text{NO}_x$ ,  $\text{SO}_2$  and  $\text{NH}_3$ . Due to the availability of favourable meteorological conditions and various anthropogenic activities (combustion, vehicular emission, etc.) for the formation of secondary aerosols at IHR, sharp peaks for  $\text{SO}_4^{2-}$ ,  $\text{NO}_3^-$  and  $\text{NH}_4^+$  in FTIR were observed in all the study sites. The strong IR

peak for  $\text{SO}_4^{2-}$  occurred at Mohal-Kullu, 613–619  $\text{cm}^{-1}$ , Almora, 615–623  $\text{cm}^{-1}$ , Nainital, 613–617  $\text{cm}^{-1}$  and Darjeeling, 611–619  $\text{cm}^{-1}$  (Anil et al. 2014; Bharti et al. 2017; Kumar et al. 2023; Pongpiachan et al. 2022; Shankar et al. 2022; Sreejith et al. 2020) due to the presence of high solar radiation, temperature and combustion-related activities that stimulate the formation of secondary sulphate ( $\text{SO}_4^{2-}$ ) through photochemical oxidation processes at the study sites (Arun et al. 2021; Chatterjee et al. 2010; Choudhary et al. 2023; Ghosh et al. 2021; Jain et al. 2019; Saraswati et al. 2019; Seinfeld and Pandis 2016). There are three IR peaks associated with  $\text{NO}_3^-$  that were shown in FTIR spectra in Mohal-Kullu (713–727  $\text{cm}^{-1}$  (sharp); 825–833  $\text{cm}^{-1}$  (weak shoulder); 1381–1404  $\text{cm}^{-1}$  (sharp)), Almora (719  $\text{cm}^{-1}$  (sharp); 827–833  $\text{cm}^{-1}$  (weak shoulder); 1381–1396  $\text{cm}^{-1}$  (sharp)), Nainital (713–721  $\text{cm}^{-1}$  (sharp); 819–821  $\text{cm}^{-1}$  (weak shoulder); 1394–1398  $\text{cm}^{-1}$  (sharp)) and two peaks in Darjeeling (717–729  $\text{cm}^{-1}$  (sharp); 1386–1398  $\text{cm}^{-1}$  (sharp)) (Anil et al. 2014; Pongpiachan et al. 2022; Shankar et al. 2022; Sreejith et al. 2020). The two weak shoulders for  $\text{NO}_2^-$  of IR vibration at Mohal-Kullu (825  $\text{cm}^{-1}$ ; 1267–1278  $\text{cm}^{-1}$ ), Almora (827  $\text{cm}^{-1}$ ; 1267–1278  $\text{cm}^{-1}$ ) and Nainital (819–821  $\text{cm}^{-1}$ ; 1274  $\text{cm}^{-1}$ ) were also reported. The increased vehicular activities stimulate the gas

**Table 2** ATR-FTIR intensity peaks ( $\text{cm}^{-1}$ ) for organic functional groups present in  $\text{PM}_{10}$  at the study sites

Functional groups	Category	Mohal-Kullu	Almora	Nainital	Darjeeling	References
Alkanes	C–I (stretching)	501–599	501–599	501–599	505–599	Cicerone (Cicerone 1981; Stuart (Stuart 2004; Merck 2023)
	C–Br (stretching)	516–698	516–688	514–696	516–694	Cicerone (1981, Stuart (2004, Merck (2023)
	C–Cl (stretching)	549–833	557–833	543–821	555–802	Cicerone (1981); Stuart (2004); Merck (2023)
	$\text{CH}_3$ and $\text{CH}_2$ deformation	1361–1479	1361–1479	1354–1473	1361–1475	Libre Texts Chemistry (2019); Shankar et al. (2023b)
	$\text{CH}_3$ , $\text{CH}_2$ and $\text{CH}$ (2 or 3 bands)	2845–3118	2845–3080	2845–3099	2845–3076	Stuart (2004); Libre Texts Chemistry (2019); Shankar et al. (2023b)
Alkenes	C=C bending (disubstituted)	667–731	669–719	669–721	650–729	Sreejith et al. (2020); Merck (2023)
	C=C stretching (monosubstituted)	1635–1647	1635–1652	1616–1622	1635–1652	Stuart (2004); Merck (2023)
	C=C (symmetry reduce intensity)	1668–1678	1678–1683	1664–1670	1662–1670	Stuart (2004); Libre Texts Chemistry (2019)
	C=C asymmetric stretch	1890–2009	1890–2015	1890–2090	1901–2002	Merck (2023)
	Allene (C=C=C stretching)	1890–2009	1901–2009	1905–2009	1901–2002	Merck (2023)
Alkynes	C–H deformation of alkynes	601–719	615–704	592–719	601–729	Libre Texts Chemistry (2019); Shankar et al. (2022); Shankar et al. (2023b)
	$\text{C}\equiv\text{C}$ symmetric stretch	2179–2409	2112–2387	2108–2360	2185–2391	Stuart (2004); Libre Texts Chemistry (2019); Shankar et al. (2022); Shankar et al. (2023b)
	C–H (usually sharp)	3273–3309	3271–3307	3275–3309	3271–3275	Stuart (2004); Libre Texts Chemistry (2019)
Cyclic rings	C–H bending and ring puckering (arenes)	682–883	686–833	688–821	694–875	Libre Texts Chemistry (2019); Shankar et al. (2022)
	Arenes (C=C (in a ring))	1506–1508	1504–1506; 1602	1506	1506–1508; 1610	Stuart (2004); Libre Texts Chemistry (2019)
Aromatic compounds	C–H bending	1651–2009	1652–1990	1651–2009	1645–2002	Stuart (2004); Merck (2023)
	Alkyl aryl ether (C–O stretching)	1267–1278	1217–1278	–	–	Stuart (2004); Merck (2023)
	Aromatic ester (C–O stretching)	1267–1319	1267–1319	1286–1319	1286–1317	Stuart (2004); Merck (2023)
	Aromatic amine (C–N stretching)	1267–1340	1267–1338	1286–1340	1286–1338	Stuart (2004); Merck (2023)



**Table 2** (continued)

Functional groups	Category	Mohal-Kullu	Almora	Nainital	Darjeeling	References
Aldehyde/Ketone/ester	Conjugated aldehyde (C=O stretching)	1681–1716	1681–1720	1681–1710	1681–1716	Stuart (2004); Merck (2023); Shankar et al. (2023b)
	Aldehyde (C=O stretching)	1716–1732	1716–1734	1716–1747	1712–1749	Stuart (2004); Merck (2023); Shankar et al. (2023b)
	C=O saturated ketones ( $\alpha$ -CH <sub>3</sub> bending)	1338–1373	1361	1340–1365	1361	Libre Texts Chemistry (2019)
	C=O saturated ketones ( $\alpha$ -CH <sub>2</sub> bending)	1390–1460	1394–1460	1394–1462	1386–1462	Libre Texts Chemistry (2019)
	Cyclopentanone (C=O stretching)	1747–1753	1747–1753	1747–1753	1747–1749	Merck (2023)
	Vinyl/phenyl ester (C=O stretching)	1768–1778	1770–1778	1770–1782	1770–1776	Stuart (2004); Merck (2023); Shankar et al. (2023b)
Alcohol/phenol	Conjugate acid halide (C=O stretching)	1768–1809	1770–1791	1770–1801	1770–1809	Merck (2023)
	O–H bending out of the plane	650–779	648–779	640–754	650–729	Stuart (2004); Libre Texts Chemistry (2019)
	O–H bending in the plane	1323–1436	1321–1438	1317–1436	1323–1436	Libre Texts Chemistry (2019); Shankar et al. (2023b)
	Alcohol (O–H stretching, intermolecular bonded)	3304–3545	3192–3556	3201–3550	3203–3543	Stuart (2004); Sreejith et al. (2020); Shankar et al. (2022); Merck (2023); Shankar et al. (2023b)
Acids	Alcohol (O–H stretching, free)	3304–3545	3564–3668	3560–3664	3545–3668	Stuart (2004); Bharti et al. (2017); Merck (2023); Shankar et al. (2023b)
	O–H bending (Carboxylic acids)	1390–1448	1386–1438	1394–1436	1394–1436	Stuart (2004); Merck (2023)
	Carboxylic acid (O–H stretching)	2845–3309	2845–3307	2845–3275	2596–3275	Stuart (2004); Merck (2023)
	Carboxylic acid (C=O stretching)	1699–1724	1681–1720	1708–1718	1712–1722	Stuart (2004); Merck (2023); Shankar et al. (2023b)
	Acids (C=O (amide I band)) N–H (2° amide)	1506–1558	1504–1558	1506–1558	1506–1558	Stuart (2004); Libre Texts Chemistry (2019)
	Acids (O–C (II band)) N–H (1° amide)	1593–1658	1602–1652	1616–1656	1606–1652	Stuart (2004); Libre Texts Chemistry (2019)
Amines	Acids	1267–1325	1217–1321	1286–1327	1286–1328	Stuart (2004); Merck (2023)
	NH <sub>2</sub> and N–H wagging (shifts on H–bonding)	650–883	655–833	655–821	655–875	Stuart (2004); Libre Texts Chemistry (2019); Shankar et al. (2023b)
	NH <sub>2</sub> scissoring (1° amine)	1541–1658	1556–1652	1550–1656	1550–1652	Stuart (2004); Libre Texts Chemistry (2019)
	Secondary amine (N–H stretching)	3332–3359	3307–3344	3305–3363	3332–3394	Stuart (2004); Merck (2023)
Aliphatic primary amine (N–H stretching)		3304–3419	3307–3410	3305–3502	3332–3502	Stuart (2004); Merck (2023); Shankar et al. (2023b)

**Table 2** (continued)

Functional groups	Category	Mohal-Kullu	Almora	Nainital	Darjeeling	References
Nitrate	Organo-nitrate	1267–1278	1267–1278	1274–1290	–	Anil et al. (2014); Bharti et al. (2017); Shankar et al. (2022)
	N–O stretching (Nitro compounds)	1487–1558	1504–1548	1483–1558	1489–1558	Stuart (2004); Merck (2023)
Hetero-compounds	C=N stretching (imine/oxime)	1641–1683	1643–1689	1633–1699	1645–1687	Stuart (2004); Merck (2023)
	Isothiocyanate (N=C=S stretching)	1990–2150	1990–2137	1984–2150	1990–2123	Merck (2023)
	Thiocyanate (S–C≡N stretching)	2144–2179	2137–2167	2146–2166	2142–2177	Shankar et al. (2022); Merck (2023); Shankar et al. (2023b)
	Carbodiimide (N=C=N stretching)	2115–2150	2112–2137	2117–2150	2115–2150	Shankar et al. (2022); Merck (2023); Shankar et al. (2023b)
	Azide (N=N=N stretching)	2115–2164	2112–2167	2117–2166	2115–2166	Shankar et al. (2022); Merck (2023); Shankar et al. (2023b)
	Nitrile (C≡N stretching)	2218–2266	2220–2268	2216–2254	2223–2250	Stuart (2004); Shankar et al. (2022); Merck (2023); Shankar et al. (2023b)
	Isocyanate (N=C=O stretching)	2252–2374	2252–2289	2245–2289	2248–2283	Shankar et al. (2022); Merck (2023); Shankar et al. (2023b)

phase conversion of  $\text{NO}_2$  to  $\text{HNO}_3$  by OH radicals, and low temperatures enhance the formation of secondary nitrate ( $\text{NO}_3^-$ ) and nitrite ( $\text{NO}_2^-$ ) by  $\text{NO}_x$  oxidation (Arun et al. 2021; Chatterjee et al. 2010; Choudhary et al. 2023; Ghosh et al. 2021; Jain et al. 2019; Saraswati et al. 2019; Seinfeld and Pandis 2016). Through association with acids such as  $\text{HNO}_3$ , HCl and  $\text{H}_2\text{SO}_4$  in the gas and aqueous phases react with gaseous and particulate  $\text{NH}_3$  ( $\text{NH}_3$  and  $\text{NH}_4^+$ ) formed the secondary inorganic aerosols ( $(\text{NH}_4)_2\text{SO}_4$ ,  $\text{NH}_4\text{NO}_3$  and  $\text{NH}_4\text{Cl}$ ) over the IHR (Sharma et al. 2014). There is abundance of ambient  $\text{NH}_3$  over the IHR produced through farming activities, raising animals, incinerating and burning activities (Sharma et al. 2014). The strong IR vibrational peaks for  $\text{NH}_4^+$  at Mohal-Kullu, 1413–1421  $\text{cm}^{-1}$ ; Almora, 1408–1419  $\text{cm}^{-1}$ ; Nainital, 1411–1421  $\text{cm}^{-1}$  and Darjeeling, 1415–1421  $\text{cm}^{-1}$  were reported (Chatterjee et al. 2010; Seinfeld and Pandis 2016; Jain et al. 2019; Saraswati et al. 2019; Sreejith et al. 2020; Ghosh et al. 2021; Arun et al. 2021; Shankar et al. 2022; Kotnala et al. 2022; Choudhary et al. 2023).  $\text{SO}_3^-$  is produced through subsequent reactions involving  $\text{H}_2\text{SO}_4$  ( $\text{SO}_2$  and OH radical primarily leads to the formation of  $\text{H}_2\text{SO}_4$ ).  $\text{H}_2\text{SO}_4$  can react with  $\text{NH}_3$  to form  $(\text{NH}_4)_2\text{SO}_4$ , which can further undergo various reactions to produce  $\text{SO}_3^-$ . The major source of  $\text{SO}_3^-$  in the air is the combustion of oil, coal and gases, which is the prominent

reason behind air pollution at study sites (Choudhary et al. 2023; Sharma et al. 2020a; Sharma et al. 2021; Yao et al. 2020). In Mohal-Kullu (975–993  $\text{cm}^{-1}$ ) and Almora (977–999  $\text{cm}^{-1}$ ), a sharp IR peak for  $\text{SO}_3^-$  was estimated.

$\text{CO}_3^{2-}$  is the main source of clay minerals like calcite, vaterite and dolomite, present in soil/road dust (Neupane et al. 2020). In Mohal-Kullu (713–721  $\text{cm}^{-1}$  (shoulder) and 1448–1462  $\text{cm}^{-1}$  (sharp)), Almora (704–719  $\text{cm}^{-1}$  (shoulder) and 1456–1462  $\text{cm}^{-1}$  (sharp)) and Nainital (713–719  $\text{cm}^{-1}$  (shoulder) and 1456  $\text{cm}^{-1}$  (sharp)), the two vibrational peaks were reported, whereas in Darjeeling, three vibrational peaks (717–727  $\text{cm}^{-1}$ , 875  $\text{cm}^{-1}$ , and 1456  $\text{cm}^{-1}$ ) for  $\text{CO}_3^{2-}$  were stated (Anil et al. 2014; Sreejith et al. 2020).

### Organic functional groups

Organic functional groups like alkanes, alkenes, alkynes, cyclic rings, aromatic compounds, carbonyl compounds, alcoholic groups, amines, organo-nitrates and some heterogeneous groups were estimated in  $\text{PM}_{10}$  for all the study sites by ATR-FTIR (Table 2). Various organic compounds like VOCs, PAHs and OC are released into the atmosphere through various anthropogenic activities like biomass burning, vehicular emissions (exhaust or non-exhaust), coal/oil/tar burning, incineration process, industrial activities and

agricultural activities (Hegde et al. 2021; Kaushal et al. 2021; Sarkar et al. 2014; Shankar et al. 2023b; Shivani et al. 2019).

Aliphatic hydrocarbons like alkanes, alkenes and alkynes were predominately detected in PM<sub>10</sub> samples at all the study sites (Table 2). The stretching frequency for alkanes (–CH<sub>3</sub>, –CH<sub>2</sub>, and –CH) was found in the range in Mohal-Kullu, 2845–3118 cm<sup>-1</sup>; Almora, 2845–3080 cm<sup>-1</sup>; Nainital, 2845–3099 cm<sup>-1</sup> and Darjeeling, 2845–3076 cm<sup>-1</sup> (Shankar et al. 2023b). For alkenes both bending and stretching (C=C bending (Mohal-Kullu, 667–731 cm<sup>-1</sup>; Almora, 669–719 cm<sup>-1</sup>; Nainital, 669–721 cm<sup>-1</sup> and Darjeeling, 650–729 cm<sup>-1</sup> (Sreejith et al. 2020) and C=C stretching (Mohal-Kullu, 1635–1647 cm<sup>-1</sup>; Almora, 1635–1652 cm<sup>-1</sup>; Nainital, 1616–1622 cm<sup>-1</sup> and Darjeeling, 1635–1652 cm<sup>-1</sup>)), IR frequencies were estimated. There is a medium intensity peak for C=C asymmetric stretch at all the study locations having frequency ranges of 1890–2009 cm<sup>-1</sup> for Mohal-Kullu, 1890–2015 cm<sup>-1</sup> for Almora, 1890–2090 cm<sup>-1</sup> for Nainital and 1901–2002 cm<sup>-1</sup> for Darjeeling (Shankar et al. 2023b). A few weak intensity broad peaks might be due to the presence of compounds having C≡C symmetric stretch in PM<sub>10</sub> samples at Mohal-Kullu (2179–2409 cm<sup>-1</sup>), Almora (2112–2387 cm<sup>-1</sup>), Nainital (2108–2360 cm<sup>-1</sup>) and Darjeeling (2185–2391 cm<sup>-1</sup>) were reported (Shankar et al. 2022; Shankar et al. 2023b). The aliphatic hydrocarbon having low as well as high molecular weight may be released in the atmosphere through vehicular exhaustion (gasoline, diesel exhaust) that might be raised due to an increase in tourist activities as all study sites are hill stations and considered to be the tourist hotspots (Sarkar et al. 2014; Shivani et al. 2019).

Several traces of cyclic rings and aromatic compounds were also detected in PM<sub>10</sub> samples in all locations. There are few medium to sharp intensity peaks of C–H bending and ring puckering detected in Mohal-Kullu (682–883 cm<sup>-1</sup>), Almora (686–833 cm<sup>-1</sup>), Nainital (688–821 cm<sup>-1</sup>) and Darjeeling (694–875 cm<sup>-1</sup>) (Shankar et al. 2022). Also, there are two sharp peaks at 1504–1506 cm<sup>-1</sup>, 1602 cm<sup>-1</sup> and 1506–1508 cm<sup>-1</sup>, 1610 cm<sup>-1</sup> in Almora and Darjeeling, respectively and only one sharp peak at 1506–1508 cm<sup>-1</sup>, and 1506 cm<sup>-1</sup> in Mohal-Kullu and Nainital corresponded to arenes (C=C). Various sharp intensity peaks ranging from 1651 to 2009 cm<sup>-1</sup> at Mohal-Kullu, 1652–1990 cm<sup>-1</sup> at Almora, 1651–2009 cm<sup>-1</sup> at Nainital and 1645–2002 cm<sup>-1</sup> at Darjeeling were observed and indicated the presence of aromatic compounds in the PM<sub>10</sub> sample. Biomass burning activities may release organic aerosols with cyclic rings (for example, levoglucosan) into the environment (Shivani et al. 2019). The major sources of aromatic compounds (PAHs) at the study sites would be gasoline-powered automobiles, diesel engine fumes, waste incineration, coal, biomass and oil/tar burning (Kaushal et al. 2021). Also, these cyclic and

aromatic ring compounds are carcinogenic and cause various adverse health impacts on the human body (Shivani et al. 2019).

The photo-oxidation of hydrocarbons or volatile organic compounds (VOCs) releases carbonyl compounds (NMVOCs) into the environment, which tend to be highly soluble in water (Hegde et al. 2021). Various IR vibrational peaks corresponding to the aldehydic (C=O stretching) group, ketonic (C=O stretching) group and ester (C=O stretching) (mostly vinyl/phenyl ester) group were observed in the FTIR spectrum of PM<sub>10</sub> samples in all the study sites. Aldehydic C=O stretching peaks in Mohal-Kullu (1716–1732 cm<sup>-1</sup>), Almora (1716–1734 cm<sup>-1</sup>), Nainital (1716–1747 cm<sup>-1</sup>) and Darjeeling (1712–1749 cm<sup>-1</sup>) were reported (Shankar et al. 2023b). However, the ketonic C=O stretching (cyclopentanone) peaks were found in Mohal-Kullu (1747–1753 cm<sup>-1</sup>), Almora (1747–1753 cm<sup>-1</sup>), Nainital (1747–1753 cm<sup>-1</sup>) and Darjeeling (1747–1749 cm<sup>-1</sup>). The vinyl/phenyl ester (C=O Stretching) IR vibrational peaks were observed in Mohal-Kullu (1768–1778 cm<sup>-1</sup>), Almora (1770–1778 cm<sup>-1</sup>), Nainital (1770–1782 cm<sup>-1</sup>) and Darjeeling (1770–1776 cm<sup>-1</sup>). These NMVOCs or carbonyl compounds are released into the environment through traffic emissions, brick kilns, biomass burning etc., and further subsidized to the formation of secondary organic aerosols (SOAs) (Sarkar et al. 2017b).

Alkanes, alkenes, aromatic rings and cyclic compounds, which have been found in the atmosphere, are photo-oxidised to produce acids, making them molecular markers or tracers for secondary volatile organic compounds (SVOCs). As a result, they can provide important information about the origin and formation pathways of aerosols. The acidity of fog, clouds and precipitation is also increased by acids (Sarkar et al. 2017a; Hegde et al. 2021). Several medium to sharp intensity IR vibrational peaks for the C=O stretching band for carboxylic acid were observed at different frequency ranges, i.e. Mohal-Kullu, 1699–1724 cm<sup>-1</sup>; Almora, 1681–1720 cm<sup>-1</sup>; Nainital, 1708–1718 cm<sup>-1</sup> and Darjeeling, 1712–1722 cm<sup>-1</sup> (Shankar et al. 2023b). Also, few weak intensity peaks for O–H stretching in carboxylic acid were detected at the frequency range in Mohal-Kullu, 2845–3309 cm<sup>-1</sup>; Almora, 2845–3307 cm<sup>-1</sup>; Nainital, 2845–3275 cm<sup>-1</sup> and Darjeeling, 2596–3275 cm<sup>-1</sup>.

The strong IR vibrational peaks for both intermolecular (Mohal-Kullu, 3304–3545 cm<sup>-1</sup>; Almora, 3192–3556 cm<sup>-1</sup>; Nainital, 3201–3550 cm<sup>-1</sup> and Darjeeling, 3203–3543 cm<sup>-1</sup>) (Shankar et al. 2022; Shankar et al. 2023b; Sreejith et al. 2020) and free O–H stretching (Mohal-Kullu, 3304–3545 cm<sup>-1</sup>; Almora, 3564–3668 cm<sup>-1</sup>; Nainital, 3560–3664 cm<sup>-1</sup> and Darjeeling, 3545–3668 cm<sup>-1</sup>) (Bharti et al. 2017; Shankar et al. 2023b) of alcohol/phenol were reported in PM<sub>10</sub> samples. Sharp peaks at frequency ranges in Mohal-Kullu, 1487–1558 cm<sup>-1</sup>; Almora, 1504–1548 cm<sup>-1</sup>; Nainital,

1483–1558  $\text{cm}^{-1}$  and Darjeeling, 1489–1558  $\text{cm}^{-1}$  which indicated the presence of N–O stretching in nitrogenous compounds. The organic aerosols having alcohol/phenol functional group tend to be known as the marker for biomass smoke plume, that in reaction with  $\text{NO}_x$  form organo-nitrate that is the tracer for biomass burning smoke (Harrison et al. 2005; Mohr et al. 2013). A weak intensity peak at intensity ranges of 1267–1278  $\text{cm}^{-1}$ , 1267–1278  $\text{cm}^{-1}$  and 1274–1290  $\text{cm}^{-1}$  in Mohal-Kullu, Almora and Nainital, respectively directed the occurrence of organo-nitrate in the analysed samples (Anil et al. 2014; Bharti et al. 2017; Shankar et al. 2022).

The nitrogen-containing heterogeneous organic aerosols (N–H stretching, C≡N stretching, C=N stretching etc.) acted as a cloud condensation nuclei (CCN). They contributed to forming SOA and light-absorbing brown carbon aerosols (Kerminen et al. 2005; Laskin et al. 2009). Various sharp peaks of N–H stretching for both primary and secondary amines were reported in Mohal-Kullu at the IR vibration range of 3304–3419  $\text{cm}^{-1}$ , in Almora at 3307–3410  $\text{cm}^{-1}$ , in Nainital at 3305–3502  $\text{cm}^{-1}$  and in Darjeeling at 3332–3502  $\text{cm}^{-1}$  (Shankar et al. 2023b). Some weak intensity overlapping peaks at Mohal-Kullu, 2218–2266  $\text{cm}^{-1}$ ; Almora, 2220–2268  $\text{cm}^{-1}$ ; Nainital, 2216–2254  $\text{cm}^{-1}$  and Darjeeling, 2223–2250  $\text{cm}^{-1}$  indicated C≡N stretching of the nitrile group present in the aerosol samples at the study sites (Shankar et al. 2022; Shankar et al. 2023b). The organic aerosols having nitrile functional group are considered to be the marker for biomass burning (wood, grasses) and burning of crop residues (Jain et al. 2023) and having amine functional group emitted specifically from industrial emissions that could be transported through air traffic mode from IGP to IHR (Jain et al. 2019; Choudhary et al. 2022; Shankar et al. 2023b). The detailed information of the wave numbers for each sample at all the study sites was given in supplementary information (Table S1–S4).

### SEM-EDX analysis

In the study,  $\text{PM}_{10}$  samples were collected from four different sampling sites: Mohal-Kullu, Almora, Nainital and Darjeeling. The samples were chosen based on their mass concentrations. The collected samples were then analysed using SEM to obtain morphology, and EDX was used to analyse the elemental composition of individual particles present in the samples. Fig. 3 represents the findings obtained from the SEM-micrographs and EDX-spectra analysis. Specifically, 105 particles from NIHE, Mohal-Kullu; 55 particles from NIHE, Almora; 116 particles from ARIES, Nainital and 54 particles from Bose Institute, Darjeeling were analysed. It has been attempted to identify the most plausible sources that may have contributed to the presence of the elements since EDX analysis provides an aw% for the identified elements.

Different elemental content during PM deposition is anticipated to contribute to various shapes. Each element's average aw% throughout the study is plotted in Fig. 4. A total of 17 elements (O, Al, Si, Na, Mg, S, Cl, K, Ca, Fe, Ba, Ti, Zn, F, Mo, Au, Zr and P) were identified through EDX scanning in each particle across all samples and study locations. The presence and frequencies of these elements provide insights into the elemental composition and the potential sources of pollutants in the  $\text{PM}_{10}$  samples (Fig. 5). The elements O, Al, Si, Na, Mg, S, Cl, K, Ca, Fe, Ba, Ti and Zn were discovered to be common in all the particles in all the locations. However, some elements, such as Mo and Au in Mohal-Kullu, F in Almora and Zr and P in Nainital, were present in extremely low frequency and were not thought to potentially contribute to the local air pollution source. It might be due to the irregularity of that specific element in samples.

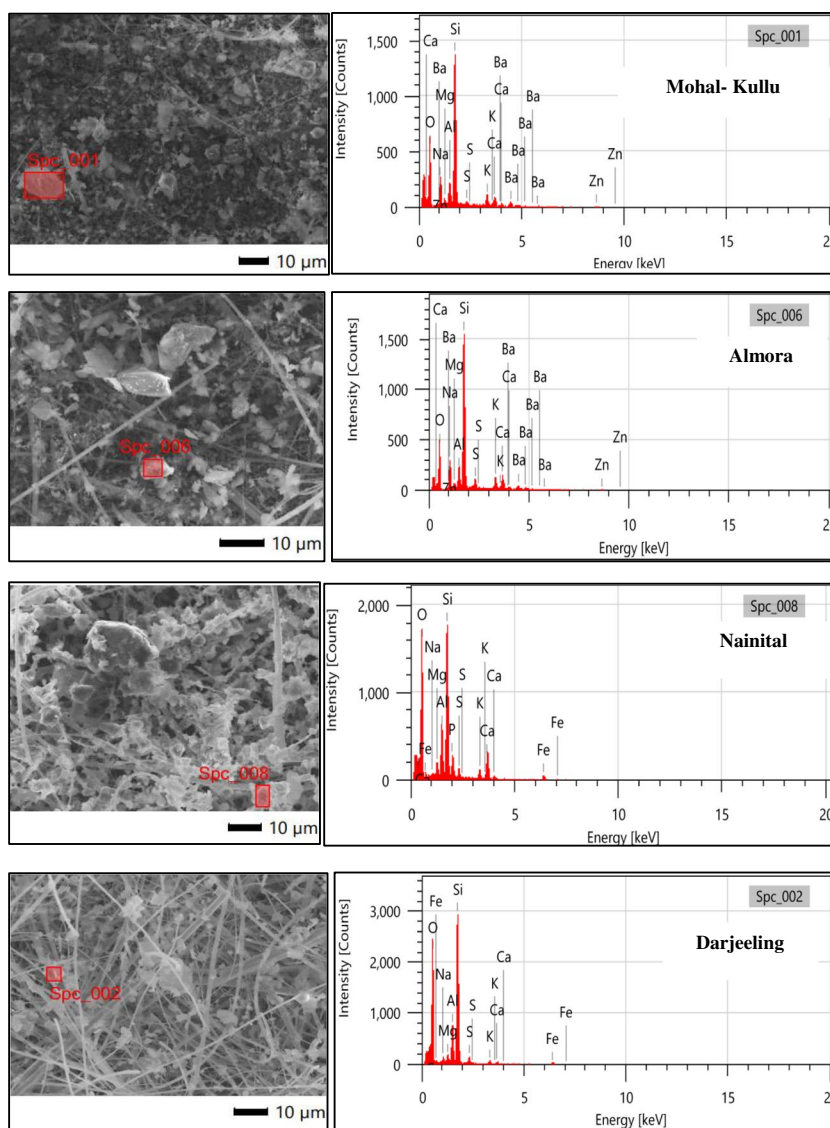
The analysis revealed that oxygen was the most enriched element in  $\text{PM}_{10}$  with average aw% of 47.72%, 45.74%, 47.99% and 47.23% at Mohal-Kullu, Almora, Nainital and Darjeeling respectively, followed by silicon (Mohal-Kullu, 22.99%; Almora, 24.46%; Nainital, 28.38% and Darjeeling, 34.08%) and aluminium (Mohal-Kullu, 6.10%; Almora, 6.31%; Nainital, 7.66% and Darjeeling, 5.16%). This enrichment pattern was observed consistently across all the studied sites. These particles were found to have irregular shapes, including columnar shapes (Mohal-Kullu), irregular solid clusters (Almora), spherical sheet-like and rod shapes (Nainital) and irregular columnar clusters (Darjeeling). According to the previous studies, the particles that are enriched with O, Si and Al with irregular and other different morphologies were found due to various natural (soil/ crustal, silica or quartz and aluminosilicates) (Bharti et al. 2017; Cong et al. 2010; Pachauri et al. 2013) as well as anthropogenic (combustion, cigarette burning, construction, etc.) activities (Khandelwal et al. 2019; Kumar et al. 2023; Murari et al. 2016).

$\text{PM}_{10}$  particles in Mohal-Kullu were enriched with elements Na (7.98%) > K (4.78%) > Ca (3.57%) > Fe (2.06%) > S (1.57%) > Ba (1.56%) > Mg (1.10%) > Zn (0.34%) > Au (0.12%) > Ti (0.06%) > Mo (0.04%) > Cl (0.04%) (Fig. 4). The particles enriched with Na, K, Fe, Ca and Mg were considered to have natural origin (crustal/soil dust/road dust) possessing spherical and irregular needle-shaped crystals, irregular solid deposition, circular disc and irregular morphology, respectively. The particles enriched with K, S and Ba comprise anthropogenic origin (combustion processes), and these particles show distinct morphological characteristics, with K-enriched particles forming irregular-shaped clusters, S-enriched particles forming solid depositions and Ba-enriched particles taking on irregular sheet-like shapes (Choudhary et al. 2022; Kuniyal and Guleria 2010).

In Almora, the  $\text{PM}_{10}$  particles exhibited primarily irregular, spherical, agglomerates, flaky, sheet-like morphology of



**Fig. 3** SEM-micrographs and their respective EDX spectra of the particles in the analysed PM<sub>10</sub> samples for all the studied sites



particles supplemented with elements, Na (5.79%) > Ca (4.27%) > K (3.44%) > Ba (3.37%) > Fe (2.49%) > S (1.57%) > Mg (1.55%) > Zn (0.78%) > Cl (0.24%) > Ti (0.11%) > F (0.10%) (Fig. 4). Among all the estimated elements, Na (spherical), Ca (irregular, spheroidal and agglomerates), K (irregular), Mg (irregular) and Fe (irregular and flaky) have crustal/soil origin. (Choudhary et al. 2023; Murari et al. 2016). The irregularly shaped particles having Ba-rich composition might be due to vehicular emissions (Labrada-Delgado et al. 2012). The particles enriched with elements such as K and S have irregular-flaky morphology and are considered the markers for biomass burning and fossil fuel burning activities (Choudhary et al. 2023; Murari et al. 2016).

Ca (2.85%) > K (2.83%) > Fe (2.80%) were the elements that were most abundant followed by Mg (1.82%) > S (1.56%) > Na (1.42%) > Ba (0.73%) > Ti (0.30%) > Zn (0.14%) > P (0.07%) > Zr (0.01%) > Cl (0.01%) in PM<sub>10</sub>

particles in Nainital (Fig. 4). In Nainital, the element Ca (irregular, spherical clusters) contributed the highest to the crustal/soil dust/road dust, followed by K (rock solid deposition-spherical), Fe (irregular deposition, needle-shaped), Na (irregular) and Mg (irregular). S (3D flaky sheet) is the highest enriched element present in the particles of PM<sub>10</sub>, followed by Ba (irregular clusters) which have an anthropogenic origin (Sharma et al. 2020a; Sheoran et al. 2021; Choudhary et al. 2022). Kimothi et al. (2023) illustrated the elements Fe, Cl, Na, K, Ca, Nb and Cl in PM<sub>2.5</sub> in the Nainital district.

PM<sub>10</sub> samples in Darjeeling were abundant with elements Na (2.74%) > K (2.51%) > Ca (2.00%) > Fe (1.83%) > S (1.64%) > Ba (1.57%) > Mg (1.01%) > Zn (0.30%) > Ti (0.03%) (Fig. 4) having particles of irregular, spherical, agglomerates and columnar morphology. Ba (irregular morphology) emitted from vehicular

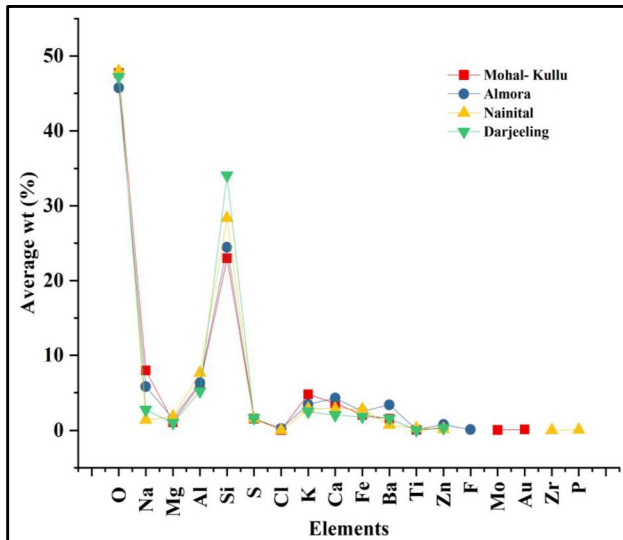


**Fig. 4** Elemental composition average aw% for representative PM<sub>10</sub> sample of each study site

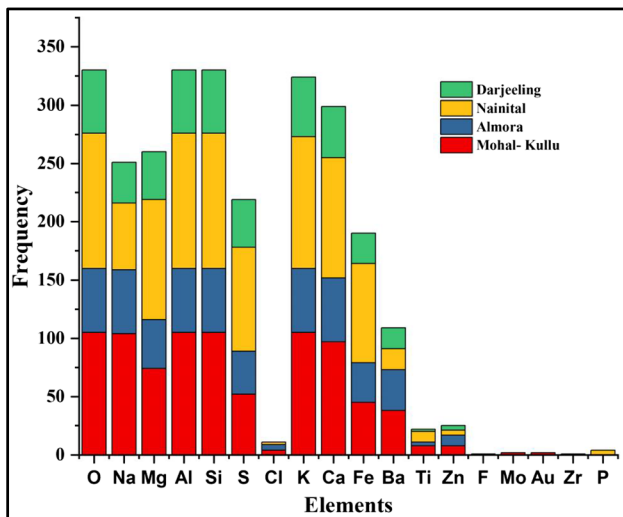


**Fig. 5** Frequency of elements in each particle of PM<sub>10</sub> samples

exhaustion enhanced due to increased tourist activities (Labrada-Delgado et al. 2012). Na (irregular), K (irregular), Ca (spherical, agglomerates), Mg (irregular) and Fe (solid deposition) have earth crust and soil dust origin (Choudhary et al. 2023; Kumar et al. 2023). The particles enriched with K and S (spherical) have an anthropogenic origin, hence emitted by combustion activities (coal combustion, biomass burning) (Adak et al. 2014; Chatterjee et al. 2021; Choudhary et al. 2023). The elements Ti and Zn were present at all study sites, but their frequencies were relatively low to consider their contribution to pollution sources (Fig. 5).

### Statistical analysis

Although common elements were estimated at all the study sites, and they corresponded to the same pollution source (whether geogenic or biogenic), the availability of each element should be site specific. Therefore, in order to test if there is an impact of various sites on the observed elemental composition, we performed ANOVA.

After applying the ANOVA separately for each element among four sites, we have observed 13 elements (O, Na, Mg, Al, Si, S, Cl, K, Ca, Fe, Ba, Ti and Zn) (Table 3), out of which eight elements (O, Mg, Cl, Ca, Fe, Ba, Ti and Zn) were found to be insignificant as their calculated *F*-test value was found to be less than *F* critical value at 5% level of significance; therefore, we accept the null hypothesis and conclude that these elements are not site-specific and we could gather the similar information about these elements from any one of the four sites.

Now, the remaining five elements (Na, Al, Si, S and K) have greater *F*-test value compared to *F* critical value at 5% level of significance; therefore, we reject the null hypothesis and conclude that there is significant difference in the mean of aw% of these elements among the four locations. Hence, the elements Na, Al, Si, S and K are site-specific in nature.

Rejecting the null hypothesis does not convey which location’s means differ from each other for the above significant elements, but it only indicated that there is a variation in at least one of the location’s means. A post hoc analysis using two sample *T*-test was conducted to determine the significance level of a specific element (detected as significant in the *F*-test) between the study sites. This test is used to compare multiple groups and identify which pairs of groups are significantly different from each other. For this, we assumed

**Table 3** *F*-test values for all the observatory sites for the estimated elements

Elements	<i>F</i> -test	<i>p</i> value	<i>F</i> critical
O	$1.6 \times 10^0$	$2.0 \times 10^{-1}$	$2.6 \times 10^0$
Na	$3.2 \times 10^1$	$1.2 \times 10^{-17}$	$2.6 \times 10^0$
Mg	$2.2 \times 10^0$	$9.3 \times 10^{-2}$	$2.6 \times 10^0$
Al	$6.4 \times 10^0$	$3.1 \times 10^{-4}$	$2.6 \times 10^0$
Si	$2.1 \times 10^1$	$1.2 \times 10^{-12}$	$2.6 \times 10^0$
S	$3.1 \times 10^0$	$2.8 \times 10^{-2}$	$2.6 \times 10^0$
Cl	$6.9 \times 10^{-1}$	$5.9 \times 10^{-1}$	$4.3 \times 10^0$
K	$2.7 \times 10^1$	$1.3 \times 10^{-10}$	$2.6 \times 10^0$
Ca	$2.4 \times 10^0$	$6.6 \times 10^{-2}$	$2.6 \times 10^0$
Fe	$2.6 \times 10^0$	$5.7 \times 10^{-2}$	$2.7 \times 10^0$
Ba	$4.5 \times 10^{-1}$	$7.1 \times 10^{-1}$	$2.7 \times 10^0$
Ti	$4.1 \times 10^{-1}$	$7.5 \times 10^{-1}$	$3.1 \times 10^0$
Zn	$4.6 \times 10^{-1}$	$7.1 \times 10^{-1}$	$3.1 \times 10^0$

that Bonferroni's correction (0.008) (Bonferroni recommended that the *p-value* for each test be equal to its  $\alpha$  value, or 5% level of confidence (0.05) divided by the number of tests, in our instance six), which is carried out when there is a multiple comparison in hypothesis testing, and the dependent variables (elemental composition) showed statistically significant results (Hayes 2021).

In this case, the *p-value* obtained from the post hoc test was compared to the Bonferroni-corrected value (0.008). If the *p-value* obtained from the post hoc test is lower than the Bonferroni-corrected value, typically considered as 0.008 in this case, it indicates that the composition of that specific element is significantly different between the study sites. For applying the post hoc test, we divide our four study sites (Mohal-Kullu, Almora, Nainital and Darjeeling) into six groups, i.e. Mohal-Kullu–Almora, Mohal-Kullu–Nainital, Mohal-Kullu–Darjeeling, Almora–Nainital, Almora–Darjeeling and Nainital–Darjeeling. In order to identify significant variations in the elements understudied, these groups provide pair-wise comparisons between the study sites (Table 4). The composition of Na was found to be similar between the Nainital-Darjeeling group but significantly different in other groups. Al composition was similar in several groups, including Mohal-Kullu-Almora, Mohal-Kullu-Darjeeling, Almora-Nainital and Almora-Darjeeling, but significantly different between Mohal-Kullu-Nainital and Nainital-Darjeeling. Si composition was similar in the Mohal-Kullu-Almora group but significantly different in other groups. S composition differed significantly in the Mohal-Kullu-Nainital group but was similar in other groups. K composition showed significant differences in several groups, including Mohal-Kullu–Almora, Mohal-Kullu–Nainital, Mohal-Kullu–Darjeeling and Almora–Darjeeling, but was similar between Almora-Nainital and Nainital-Darjeeling. These findings highlight variations in elemental composition among different groups within the study sites for Na, Al, Si, S and K in PM<sub>10</sub> particles.

## Potential sources and source regions

### Potential source identification using PCA and enrichment factor

The enrichment factor (EF) facilitates the differentiation of elements sourced from natural and man-made sources. An origin for soil or crustal particulates that is primarily natural is suggested when EF is less than 5. An EF between 5 and 10 denotes a combination of human and natural sources. A predominantly anthropogenic origin, frequently linked to human activity, is indicated by EF values greater than 10 (Sharma et al. 2014). In the present study, the analysis shows that elements (Na, Fe, K, Mg, Ti, Ca and K) with EF values less than 5 are probably from natural crustal origin. Conversely, Ti also have EF values ranging from 5 to 10, indicating that a combination of both human activity as well as from natural processes, specifically combustion, building or destruction, etc., is their source. EF values more than 10 clearly indicate that the origin of elements like Zn, Mo, Zr and P is primarily anthropogenic most likely result from vehicular emissions and human activities (Fig. S2, in supplementary information).

In conducting the PCA analysis for this study, IBM's SPSS software version 26.0 was employed. Primarily dust aerosols, combustion-related activities and vehicular emission are evaluated as the major contributor at all study sites (Fig. S3, in supplementary information). The possible sources extracted by PCA over the study sites are discussed below.

**Mohal-Kullu** In Mohal-Kullu, four sources of particulate aerosols were evaluated by using PCA which mainly includes the elements Na, Al, S, Mg, Ca, Ba, Si, K and Fe. Soil dust, resuspended dust, paved road dust and a mixed source (coal fly ash + resuspended traffic dust + construction) were identified as major contributor to particulate matter (Choudhary et al. 2022; Jangirh et al. 2022; Karaca et al. 2019; Kaushal et al. 2018; Shashni et al. 2018).

**Table 4** *p* value test for the significant elements between the study sites

Elements	Mohal-Kullu-Almora	Mohal-Kullu-Nainital	Mohal-Kullu-Darjeeling	Almora-Nainital	Almora-Darjeeling	Nainital-Darjeeling
Na	$9.3 \times 10^{-6}$	$4.7 \times 10^{-16}$	$4.1 \times 10^{-8}$	$1.6 \times 10^{-8}$	$6.4 \times 10^{-3}$	$3.5 \times 10^{-2}$
Al	$6.9 \times 10^{-1}$	$5.1 \times 10^{-3}$	$1.1 \times 10^{-1}$	$9.7 \times 10^{-3}$	$4.1 \times 10^{-2}$	$3.0 \times 10^{-5}$
Si	$2.4 \times 10^{-1}$	$1.4 \times 10^{-5}$	$3.4 \times 10^{-11}$	$3.7 \times 10^{-3}$	$2.1 \times 10^{-8}$	$3.8 \times 10^{-4}$
S	$2.2 \times 10^{-1}$	$3.5 \times 10^{-3}$	$1.1 \times 10^{-2}$	$6.2 \times 10^{-1}$	$7.8 \times 10^{-1}$	$6.2 \times 10^{-1}$
K	$3.4 \times 10^{-7}$	$1.3 \times 10^{-11}$	$9.7 \times 10^{-11}$	$1.6 \times 10^{-2}$	$4.2 \times 10^{-3}$	$3.7 \times 10^{-1}$

**Almora** In Almora, there were three sources estimated with the help of PCA which includes the elements Si, Ca, Mg, Al, K, Na, Ba, Fe and S. The types of sources identified at this site contain crustal dust, fuel combustion, ash fraction of diesel exhaust + markers of brake wear which mainly contributed to the particulate aerosol's concentration (Sharma et al. (2020a); Karaca et al. 2019; Choudhary et al. 2022).

**Nainital** In Nainital also, there were four sources evaluated by PCA which contains elements majorly Mg, Fe, Si, K, Al, Ca, S, Na and Ba. The types of sources that were estimated at Nainital include soil dust, crustal dust + ash fraction of diesel exhaust and markers of brake wear, paved road dust + coal combustion, crustal dust + brake wear and tear from motor vehicles (Sharma et al. (2020a); Karaca et al. 2019; Sheoran et al. 2021; Jangirh et al. 2022; Choudhary et al. 2022).

**Darjeeling** Like as in Nainital, it also has four identified sources which include elements mainly Al, K, Si, Mg, Ca, S, Na, Ba and Fe. Ash fractions of diesel exhausts + markers of brake wear, resuspended dust, soil dust and brake wear and tear from motor vehicles were the major type of sources that contributed mainly in the particulate concentration of this study site (Chatterjee et al. 2010, 2021; Karaca et al. 2019; Shivani et al. 2019; Sharma et al. (2020b); Jangirh et al. 2022; Choudhary et al. 2022).

### Impact of air parcel trajectory on PM<sub>10</sub>

To comprehend the trajectories of particulate air masses reaching the sampling sites (Mohal-Kullu, Almora, Nainital and Darjeeling), we generated annual trajectories at 500m AGL illustrated in the Fig. 6a. The annual trajectories for all locations primarily originated from local regions such as Uttarakhand, Jammu and Kashmir, the Thar Desert, Himachal Pradesh, Afghanistan, the Indo-Gangetic Plain (IGP) region and the Bay of Bengal (BoB).

The atmospheric mass backward trajectories reaching Mohal-Kullu had their origins in the IGP region, Afghanistan, Pakistan and some traversing over the Arabian Sea. Also, substantial air mass loadings were observed, predominantly originating from northwestern countries such as Turkmenistan, Afghanistan and Pakistan (Choudhary et al. 2022; Gajananda et al. 2005). The backward trajectory reaching Almora primarily originated from IGP region including the arid regions of the western part of India, Afghanistan and Pakistan. In Nainital, the air parcel had their origins in Pakistan, Afghanistan, Iran, the Thar Desert and the IGP region of India (Choudhary et al. 2022; Sharma et al. 2021). The substantial influx of backward trajectories reaching Darjeeling can be traced back to origins in the dry lands, including the Thar Desert, Rajasthan and Punjab, as well as the IGP region, Bay of Bengal (BoB), Assam, Sikkim and Nepal

(Chatterjee et al. 2021; Choudhary et al. 2022; Rai et al. 2020, 2021).

To pinpoint the potential source regions of PM<sub>10</sub> at the receptor sites (Mohal-Kullu, Almora, Nainital, and Darjeeling), a PSCF analysis was performed. Grids with a probability below 0.1 are rendered transparent, while other grids are displayed in various colours, where lighter shades indicate lower probabilities and darker hues signify higher probabilities. In Mohal-Kullu, substantial air mass loads from the north originated in Jammu and Kashmir, while those from the south-east came from Uttarakhand regions (Choudhary et al. 2022) (Fig. 6b). In Almora, heightened loads were locally sourced from Uttarakhand and north-westward from Himachal Pradesh (Fig. 6c). Nainital experienced heavy loads from local sources in Uttarakhand, north-westward from Himachal Pradesh and certain regions of Nepal (Sharma et al. 2021; Sheoran et al. 2021) (Fig. 6d). In Darjeeling, contributions to the heavy loading of particulate aerosols came from Nepal, Bhutan, Sikkim, Kolkata and some areas of Bihar (Ghosh et al. 2021; Rai et al. 2020, 2021) (Fig. 6e).

### CBPF

The predominant long-range transport of air parcels towards the IHR is influenced by sources within the regional and trans-boundary areas, particularly in the west (W), south (S), northwest (N-W), southwest (S-W) and southeast (S-E) directions. Regions such as Uttarakhand, Jammu and Kashmir, the Thar Desert, Himachal Pradesh, Pakistan, Afghanistan, Nepal, Sikkim, the IGP and the BoB contribute to the increased loading of atmospheric pollutants in various locations within the IHR. To better understand the directionality of local sources, a CBPF plot was performed for Mohal-Kullu, Nainital and Darjeeling (except Almora due to unavailability of met data).

**Mohal-Kullu** With > 75th percentile of mass concentration ( $63 \mu\text{g m}^{-3}$ ) and the WS  $\sim (0.3\text{--}0.8 \text{ m s}^{-1})$ . CBPF for Mohal-Kullu directs the source in the local region N-W and S-W could be considered as plausible contributors to the mass loading observed at the site. (Fig. 7a) Highly dense areas covered by tourist hotspots like Solan (S-W), Mandi (N-W) and Bilaspur (W) lead to the traffic influx which could be the possible source emitter towards the site.

**Nainital** With > 75th percentile of mass concentration ( $67 \mu\text{g m}^{-3}$ ) and the WS  $\sim (0.5\text{--}3.5 \text{ m s}^{-1})$ . The CBPF for Nainital suggests that potential sources within the local region to the N-W, S-W and S-E could be considered as conceivable factors contributing to the mass loading at the site (Fig. 7b). The particulate air parcel coming from N-W and S-W directions majorly transport from nearby IGP region (Choudhary et al. 2022, Sharma et al. 2021).



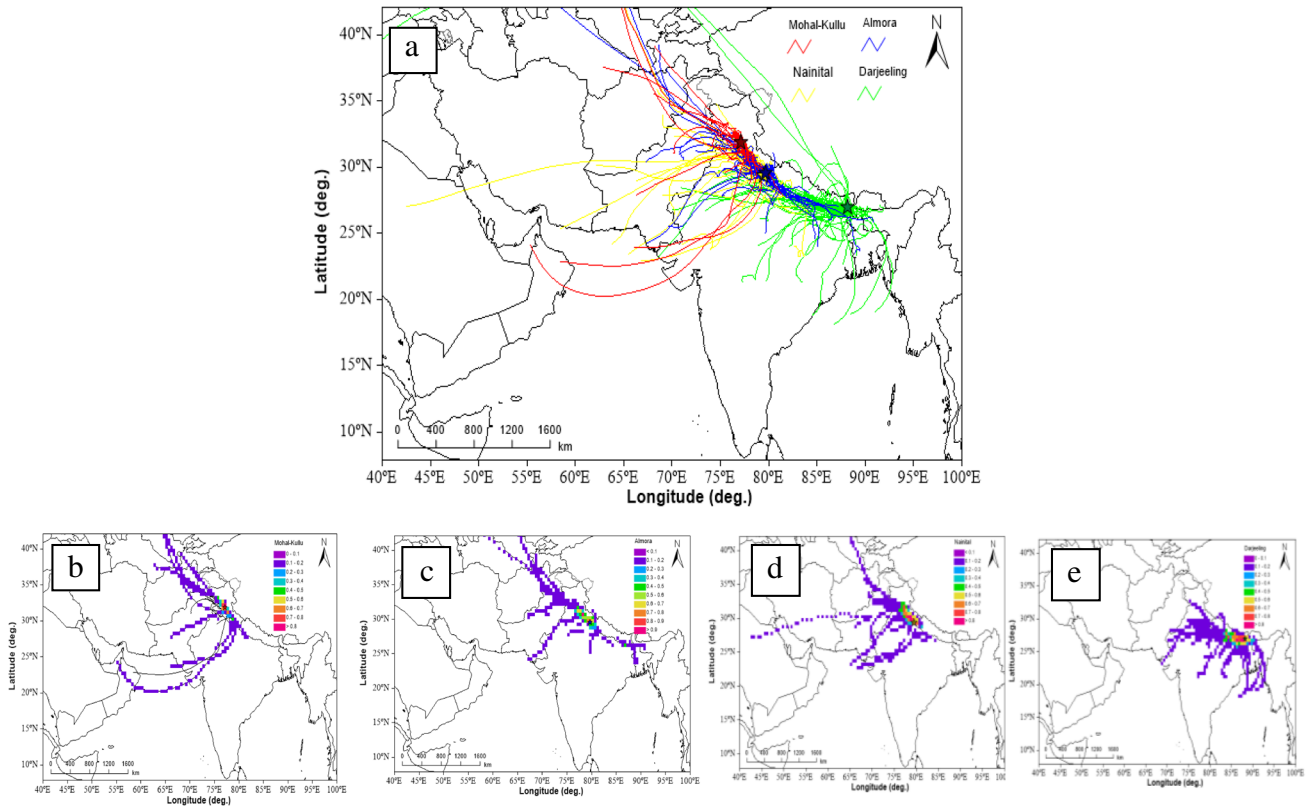


**Fig. 6** Air mass backward trajectories (a Mohal-Kullu, Almora, Nainital, and Darjeeling) and PSCF (Mohal-Kullu (b), Almora (c), Nainital (d) and Darjeeling (e)) of  $PM_{10}$  at height 500 m (AGL) over IHR

**Darjeeling** With > 75th percentile of mass concentration ( $55 \mu g m^{-3}$ ) and the WS  $\sim (0.2-1.4 m s^{-1})$ . CBPF for Darjeeling directs the source in the local region S-W, and S-E could be plausible cause for mass loading at the site (Fig. 7c). The particulate air parcel coming from S-W and SE directions majorly transport from anthropogenic emissions from IGP specifically Kolkata region (Choudhary et al. 2022).

**Conclusion**

The present study inferred the annual average concentration of  $PM_{10}$ , their morphological characteristics with elemental content and their IR spectra over the IHR. It is the first attempt to assess the FTIR spectral analyses and SEM-EDX analyses simultaneously of the  $PM_{10}$  over IHR. The findings suggested that in Almora and Darjeeling, the pollution load of  $PM_{10}$  was

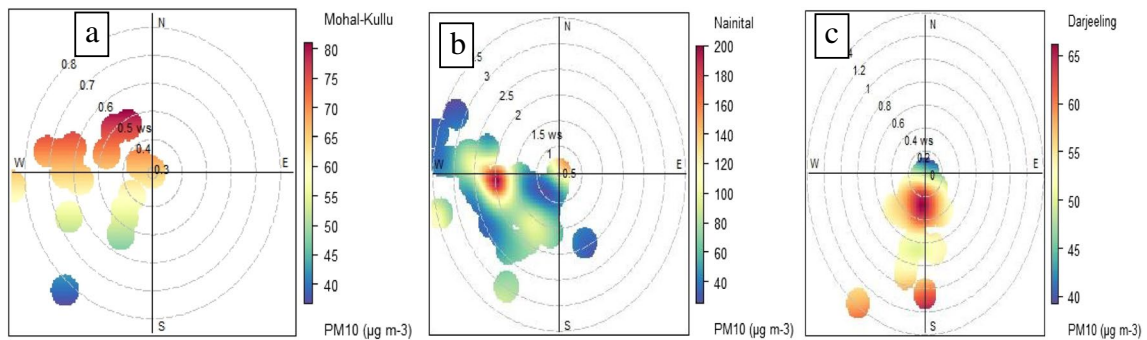


**Fig. 7** CBPF plots  $PM_{10}$  concentration at the receptor sites (a) Mohal-Kullu, (b) Nainital, (c) Darjeeling) over IHR

within the permissible limit of NAAQS; however Nainital and Mohal-Kullu have higher level of  $PM_{10}$ . The ATR-FTIR spectral analysis revealed the presence of inorganic ions, which can be attributed to various geogenic activities and secondary atmospheric reactions. Additionally, the analysis detected organic functional groups that are associated with both biogenic and anthropogenic sources of pollution. These findings indicate the complex nature of the pollutants present in  $PM_{10}$ , with contributions from natural and human-induced sources. SEM-EDX analyses inferred that the elements having natural origin (Al, Na, K, Ca, Mg and Fe) have variable (irregular, spherical, cluster, sheet-like solid deposition, columnar) morphology, whereas anthropogenic origin (K, S and Ba) has mostly irregular and spherical morphology at all the study sites. The composition of O, Si and Al in elemental form and the sharp peak of the silicate ion in the ATR-FTIR spectra corroborated the presence of aluminosilicate in  $PM_{10}$  samples at all of the study sites, demonstrating the complementary nature of the two techniques. Additionally, the presence of  $SO_4^{2-}$  and  $CO_3^{2-}$  ion peaks in the IR spectra and the Ca enrichment in the particle at all sites with natural origin highlighted the presence of  $CaSO_4$  and  $CaCO_3$  in the  $PM_{10}$  samples at all sampling locations. The statistical analysis ANOVA explained that the means of aw% of elements Na, Al, Si, S and K are significantly different and varied from one site to another. Also, PCA inferred that predominantly dust aerosols, combustion-related activities and vehicular emissions are the primary sources of atmospheric pollutants at all study sites. Trajectory analysis indicated that increased levels of pollutants in different locations within the IHR can be attributed to contributions from Uttarakhand, Jammu and Kashmir, the Thar Desert, Himachal Pradesh, Pakistan, Afghanistan, Nepal, Sikkim, the IGP and the BoB. Overall, the work sheds insight into the characteristics, elemental composition and IR spectra of  $PM_{10}$  in the IHR and emphasises the benefits of integrating FTIR and SEM-EDX analysis to thoroughly comprehend the  $PM_{10}$  pollution in the region.

**Supplementary Information** The online version contains supplementary material available at <https://doi.org/10.1007/s11356-024-31973-3>.

**Acknowledgements** The authors (SKS, SG, NC, AR) are thankful to Director, CSIR-NPL, and Head, Environmental Sciences and Biomedical Metrology Division (ES&BMD), CSIR-NPL, New Delhi, for their encouragement and support for this study. The authors SS and RG acknowledge sincere gratitude to the Vice Chancellor, Indira Gandhi Delhi Technical University for Women, New Delhi, for fostering R&D collaborations and providing analytical facilities. The authors JCK, RL, SC, IT, AB and ST heartily thank the Director of G. B. Pant National Institute of Himalayan Environment, Kosi-Katarmal, Almora, India, for providing facilities and encouraging inter-institutional R&D activities. They are thankful to ISRO for providing partial financial assistance to carry out the present study under Aerosol Radiative Forcing over India (ARFI) under ISRO-GBP. The authors thankfully acknowledge the NOAA Air Resources Laboratory for downloading the air mass trajectories (<http://www.arl.noaa.gov/ready/hysplit4.html>) datasets.

**Author contribution** Sakshi Gupta: conceptualization, design of the study, data analysis, visualization, original draft-writing, and editing; Shobhna Shankar: sample analysis, editing, and reviewing; Jagdish Chandra Kuniyal: data interpretation, developed hypothesis, data analysis, editing and reviewing; Priyanka Srivastava: sample collection, editing and reviewing; Renu Lata: Sample collection, developed hypothesis, data analysis, editing and reviewing; Sheetal Chaudhary: sample collection, editing, and reviewing; Isha Thakur: sample collection, editing, and reviewing; Archana Bawari: sample collection, editing, and reviewing; Shilpa Thakur: Sample collection, editing, and reviewing; Momani Dutta: sample collection, editing, and reviewing; Abhinandan Ghosh: sample collection, editing, and reviewing; Manish Naja: Data interpretation, developed hypothesis, data analysis, editing and reviewing; Abhijeet Chatterjee: data interpretation, developed hypothesis, data analysis, editing and reviewing; Ranu Gadi: data interpretation, developed hypothesis, data analysis, editing and reviewing; Nikki Choudhary: Data collection, Editing and Reviewing; Akansha Rai: data collection, editing and reviewing; Sudhir Kumar Sharma: conceptualization and design of the study, data interpretation, writing, editing and reviewing. All authors have read and agreed to the published version of the manuscript.

**Funding** The Department of Science and Technology (DST), Government of India, New Delhi, India, provided financial support for this study (SKS, SG, AR) (DST/CCP/Aerosol/88/2017). The DST, New Delhi, provided research fellowship (NC).

**Data availability** The datasets developed during the current study are available from the corresponding author on reasonable request.

## Declarations

**Ethical approval** Not applicable.

**Consent to participate** Not applicable.

**Consent for publication** Not applicable.

**Competing interests** The authors declare no competing interests.

## References

- Adak A, Chatterjee A, Singh AK, Sarkar C, Ghosh S, Raha S (2014) Atmospheric fine mode particulates at Eastern Himalaya, India: role of meteorology, long-range transport and local anthropogenic sources. *Aerosol Air Qual Res* 14:440–450. <https://doi.org/10.4209/aaqr.2013.03.0090>
- Aggarwal RK, Chandel SS (2010) Emerging energy scenario in Western Himalayan state of Himachal Pradesh. *Energy Policy* 38:2545–2551. <https://doi.org/10.1016/j.enpol.2010.01.002>
- Anil I, Alagha O (2020) Source apportionment of ambient black carbon during the COVID-19 lockdown. *Int J Environ Res Public Health* 17:9021. <https://doi.org/10.3390/ijerph17239021>
- Anil I, Alagha O, Blais NI, Mohamed IA, Barghouthi MH, Manzar MS (2019) Source identification of episodic rain pollutants by a new approach: combining satellite observations and backward air mass trajectories. *Aerosol Air Qual Res* 19:2827–2843. <https://doi.org/10.4209/aaqr.2019.04.0187>
- Anil I, Golcuk K, Karaca F (2014) ATR-FTIR spectroscopic study of functional groups in aerosols: the contribution of a Saharan dust transport to urban atmosphere in Istanbul, Turkey. *Water Air Soil Pollut* 225:1898. <https://doi.org/10.1007/s11270-014-1898-9>

- Arun BS, Gogoi MM, Hegde P, Borgohain A, Boreddy SKR, Kundu SS, Babu SS (2021) Carbonaceous aerosols over Lachung in the Eastern Himalayas: primary sources and secondary formation of organic aerosols in a remote high-altitude environment. *ACS Earth and Space Chem* 5(9):2493–2506. <https://doi.org/10.1021/acsearthsp.acechem.1c00190>
- Begam GR, Vachaspati CV, Ahammed YN, Kumar KR, Reddy RR, Sharma SK, Saxena M, Mandal TK (2017) Seasonal characteristics of water-soluble inorganic ions and carbonaceous aerosols in total suspended particulate matter at a rural semi-arid site, Kadapa (India). *Environ Sci Pollut Res Int* 24(2):1719–1734. <https://doi.org/10.1007/s11356-016-7917-1>
- Belis CA, Karagulian F, Larsen BR, Hopke PK (2013) Critical review and meta-analysis of ambient particulate matter source apportionment using receptor models in Europe. *Atmos Environ* 69:94e108. <https://doi.org/10.1016/j.atmosenv.2012.11.009>
- Bharti SK, Kumar D, Anand S, Poonam, Barman SC, Kumar N (2017) Characterization and morphological analysis of individual aerosol of PM<sub>10</sub> in urban area of Lucknow, India. *Micron* 103:90–98. <https://doi.org/10.1016/j.micron.2017.09.004>
- Bond TC, Doherty SJ, Fahey DW, Forster PM, Bernsten T, DeAngelo BJ, Flanner MG, Ghan S, Karcher B, Koch D (2013) Bounding the role of black carbon in the climate system: a scientific assessment. *J Geophys Res Atmos* 118:5380–5552. <https://doi.org/10.1002/jgrd.50171>
- Chatterjee A, Adak A, Singh A, Srivastava M, Ghosh S, Tiwari S, Devara P, Raha S (2010) Aerosol chemistry over a high-altitude station at north-eastern Himalayas, India. *PLoS One* 5(6):e11122. <https://doi.org/10.1371/journal.pone.0011122>
- Chatterjee A, Mukherjee S, Dutta M, Ghosh A, Ghosh SK, Roy A (2021) High rise in carbonaceous aerosols under very low anthropogenic emissions over eastern Himalaya, India: Impact of lockdown for COVID-19 outbreak. *Atmos Environ* 244:117947. <https://doi.org/10.1016/j.atmosenv.2020.117947>
- Cheng WC, Liu CH, Leung DY (2009) On the correlation of air and pollutant exchange for street canyons in combined wind-buoyancy-driven flow. *Atmos Environ* 43:3682–3690. <https://doi.org/10.1016/j.atmosenv.2009.04.054>
- Cheng WL, Chen YS, Zhang J, Lyons TJ, Pai JL, Chang SH (2007) Comparison of the Revised Air Quality Index with the PSI and AQI indices. *Sci Total Environ* 382(2-3):191–198. <https://doi.org/10.1016/j.scitotenv.2007.04.036>
- Choudhary N, Rai A, Kuniyal JC, Srivastava P, Lata R, Dutta M, Ghosh A, Dey S, Sarkar S, Gupta S, Chaudhary S, Thakur I, Bawari A, Naja M, Vijayan N, Chatterjee A, Mandal TK, Sharma SK, Kotnala RK (2023) Chemical characterization and source apportionment of PM<sub>10</sub> using receptor models over the Himalayan Region of India. *Atmosphere* 14:880. <https://doi.org/10.3390/atmos14050880>
- Choudhary N, Srivastava P, Dutta M, Mukherjee S, Rai A, Kuniyal JC, Lata R, Chatterjee A, Naja M, Vijayan N, Mandal TK, Sharma SK (2022) Seasonal characteristics, sources and pollution pathways of PM<sub>10</sub> at high altitudes Himalayas of India. *Aerosol Air Qual Res* 22(7). <https://doi.org/10.4209/aaqr.220092>
- Cicerone RJ (1981) Halogens in atmosphere. *Rev Geophys And Space Phys* 19:123–139
- Colonna KJ, Kotrakakis P, Kinney PL, Cooke RM, Evans JS (2022) Mortality attributable to long-term exposure to ambient fine particulate matter: insight from the epidemiologic evidence for understudied locations. *Environ Sci Technol* 56(11):6799–6812. <https://doi.org/10.1021/acs.est.1c08343>
- Cong Z, Kang S, Dong S, Liu X, Qin D (2010) Elemental and individual particle analysis of atmospheric aerosols from high Himalayas. *Environ Monit Assess* 160:323–335. <https://doi.org/10.1007/s10661-008-0698-3>
- Davies T, Cahill S (2000) Environmental implications of the tourism industry. Discussion paper 00-14, Resources for the Future, NW Washington, DC, p 20036
- Dockery DW, Pope CA, Xu X, Spengler JD, Ware JH, Fay ME, Ferris BG, Speizer FE (1993) An association between air pollution and mortality in six US cities. *New Engl J Med* 329(24):1753–1759. <https://doi.org/10.1056/NEJM199312093292401>
- Gajananda K, Kuniyal JC, Momin G, Pasmarti R, Safai P, Tiwari S, Ali K (2005) Trend of atmospheric aerosols over the north western Himalayan region, Inida. *Atmos Environ* 39:4817–4825. <https://doi.org/10.1016/j.atmosenv.2005.01.038>
- Ghosh A, Patel A, Rastogi N, Sharma SK, Mandal T, Chatterjee A (2021) Size-segregated aerosols over a high-altitude himalayan and a tropical urban metropolis in Eastern India: chemical characterization, light absorption, role of meteorology and long-range transport. *Atmos Environ* 254:118398. <https://doi.org/10.1016/j.atmosenv.2021.118398>
- Guleria RP, Kuniyal JC, Sharma NL, Dhyani PP (2012) Seasonal variability in aerosol optical and physical characteristics estimated using the application of the Ångström formula over Mohal in the north-western Himalaya, Inida. *J Earth Syst Sci* 121:697–710. <https://doi.org/10.1007/s12040-012-0194-6>
- Gupta S, Gadi R, Sharma SK, Mandal TK (2018) Characterization and source apportionment of organic compounds in PM<sub>10</sub> using PCA and PMF at a traffic hotspot of Delhi. *Sustain Cities Soc* 39:52–67. <https://doi.org/10.1016/j.scs.2018.01.051>
- Gupta S, Sharma SK, Mandal TK (2023) Elemental analysis and health risk assessment of PM<sub>2.5</sub> at an urban site of Delhi. Chapter 16, Recent Advances in Metrology. In: Yadav S, Garg N, Aggarwal SG, Jaiswal SK, Kumar H (eds) Venu Gopal Achanta. Springer Science and Business Media
- Harrison MAJ, Barra S, Borghesi D, Vione D, Arsene C, Iulian Olariu R (2005) Nitrated phenols in the atmosphere: a review. *Atmos Environ* 39:231–248. <https://doi.org/10.1016/j.atmosenv.2004.09.044>
- Hayes A (2021) What is the Bonferroni test (correction) and how it is used. *Fundamental Analysis, Investopedia*
- Hegde P, Boreddy SKR, Aswini AR, Aryasree S (2021) Influence of south Asian outflow on secondary organic aerosol formation over the Indian Ocean: inferences from water-soluble low molecular weight dicarboxylic acids and related organic compounds during ICARB 2018 experiment. *Mar Chem* 239:104071. <https://doi.org/10.1016/j.marchem.2021.104071>
- Indian Minerals Yearbook 2018 (Part-III: Mineral Reviews). Ilmenite and Rutile, Government of India ministry of mines Indian Bureau of Mines; 57<sup>th</sup> Edition. [www.ibm.gov.in](http://www.ibm.gov.in)
- Jain S, Sharma SK, Srivastava MK, Chatterjee A, Singh RK, Saxena M, Mandal TK (2019) Source apportionment of PM<sub>10</sub> over three tropical urban atmospheres at Indo-Gangetic Plain of India: an approach using different receptor models. *Arch Environ Contam Toxicol* 76(1):114–128. <https://doi.org/10.1007/s00244-018-0572-4>
- Jain S, Sharma SK, Vijayan N (2020) Seasonal characteristics of aerosols (PM<sub>2.5</sub> and PM<sub>10</sub>) and their source apportionment using PMF: a four-year study over Delhi, India. *Environ Pollut* 262:114337. <https://doi.org/10.1016/j.envpol.2020.114337>
- Jain S, Sharma SK, Vijayan N (2021) Investigating the seasonal variability in source contribution to PM<sub>2.5</sub> and PM<sub>10</sub> using different receptor models during 2013–2016 in Delhi, India. *Environ Sci Pollut Res* 28:4660–4675. <https://doi.org/10.1007/s11356-020-10645-y>
- Jain V, Tripathi N, Tripathi SN, Gupta M, Sahu LK, Murari V, Gaddamidi S, Shukla AK, Prevot ASH (2023) Real-time measurements of non-methane volatile organic compounds in the central Indo-Gangetic basin, Lucknow, India: source characterisation and their role in O<sub>3</sub> and secondary organic aerosol formation. *Atmos Chem Phys* 23:3383–3408. <https://doi.org/10.5194/acp-23-3383-2023>
- Jangirh R, Ahlawat S, Arya R, Mondal A, Yadav L, Kotnala G, Yadav P, Choudhary N, Rani M, Banoo R, Rai A, Saharan US, Rastogi N,



- Patel A, Shivani, Gadi R, Saxena P, Vijayan N, Sharma C, Sharma SK (2022) Gridded distribution of total suspended particulate matter (TSP) and their chemical characterization over Delhi during winter. *Environ Sci Pollut Res* 29:17892–17918. <https://doi.org/10.1007/s11356-021-16572-w>
- Jerrett M (2015) The death toll from air-pollution sources. *Nature* 525(7569):330–331. <https://doi.org/10.1038/525330a>
- Joshi P, Dey S, Ghosh S, Jain S, Sharma SK (2022) Association between acute exposure to PM<sub>2.5</sub> chemical species and mortality in megacity Delhi, India. *Environ Sci Technol* 56:7275–7287. <https://doi.org/10.1021/acs.est.1c06864>
- Karaca F, Anil I, Yildiz A (2019) Physicochemical and morphological characterization of atmospheric coarse particles by SEM/EDS in new urban central districts of a megacity. *Environ Sci Pollut Res Int* 26(23):24020–24033. <https://doi.org/10.1007/s11356-019-05762-2>
- Kaushal D, Bamotra S, Yadav S, Chatterjee S, Tandon A (2021) Particulate bound polycyclic aromatic hydrocarbons over Dhauladhar region of the north-western Himalayas. *Chemosphere* 263:128298. <https://doi.org/10.1016/j.chemosphere.2020.128298>
- Kaushal D, Kumar A, Yadav S, Tandon A, Attri AK (2018) Wintertime carbonaceous aerosols over Dhauladhar region of North-Western Himalayas. *Environ Sci Pollut Res* 25:8044–8056. <https://doi.org/10.1007/s11356-017-1060-5>
- Kerminen VM, Lihavainen H, Komppula M, Viisanen Y, Kulmala M (2005) Direct observational evidence linking atmospheric aerosol formation and cloud droplet activation. *Geophys Res Lett* 32:1–4. <https://doi.org/10.1029/2005GL023130>
- Khandelwal N, Tiwari R, Saini R, Taneja A (2019) Particulate and trace metal emission from mosquito coil and cigarette burning in environmental chamber. *SN Appl Sci* 1:441. <https://doi.org/10.1007/s42452-019-0435-2>
- Kimothi S, Chilkoti S, Rawat V, Thapiyal A, Gautam AS, Gautam S (2023) Micro- to macro-scaling analysis of PM<sub>2.5</sub> in sensitive environment of Himalaya, India. *Geol J*:1–19. <https://doi.org/10.1002/gj.4765>
- Kotnala G, Sharma SK, Mandal TK (2022) Long-Term (2013–2018) Relationship of water-soluble inorganic ionic species of PM<sub>2.5</sub> with ammonia and other trace gases in Delhi, India. *Aerosol Sci Eng* 6(4):349–359. <https://doi.org/10.1007/s41810-022-00154-5>
- Kumar A, Attri AK (2016) Biomass combustion a dominant source of carbonaceous aerosols in the ambient environment of western Himalayas. *Aerosol Air Qual Res* 16(3):519–529. <https://doi.org/10.4209/aaqr.2015.05.0284>
- Kumar S, Bharti SK, Kumar N (2023) Diurnal and seasonal variation in morphology and elemental composition of particulate matters. *J Geol Soc India* 99:666–674. <https://doi.org/10.1007/s12594-023-2367-0>
- Kumar S, Jain MK (2022) Characterization and morphometric study of household settled dust: a case study in Dhanbad, the coal capital of India. *Appl Geochem* 144(105398). <https://doi.org/10.1016/j.apgeochem.2022.105398>
- Kumar UD (2017) Chapter-7, analysis of variance, business analytics: The science of data-driven decision making. Wiley, pp 189–205
- Kuniyal JC, Guleria R (2010) Aerosols optical properties prone to climate change over Mohal-Kullu in the northwestern Himalaya, India. In: Conference of Indian Aerosol Science and Technology Association on: Aerosols and clouds: Climate Change perspective. Bose institute Darjeeling, India. March 24–26, 19(1 and 2), pp 227–230
- Labrada-Delgado G, Aragon-Pina A, Campos-Ramos A, Castro-Romero T, Amador-Munoz O, Villalobos-Pietrin R (2012) Chemical and morphological characterization of PM<sub>2.5</sub> collected during MILA-GRO campaign using scanning electron microscopy. *Atmos Poll Res* 3:289–300. <https://doi.org/10.5094/APR.2012.032>
- Larkin PJ (2018) Chapter 6-IR and Raman spectra–structure correlations: characteristic group frequencies, infrared and Raman spectroscopy, second edn. Elsevier, pp 85–134. <https://doi.org/10.1016/B978-0-12-804162-8.00006-9>
- Laskin A, Smith JS, Laskin J (2009) Molecular characterization of nitrogen-containing organic compounds in biomass burning aerosols using high-resolution mass spectrometry. *Environ Sci Technol* 43:3764–3771. <https://doi.org/10.1021/es803456n>
- Lelieveld J, Evans JS, Fnais M, Giannadaki D, Pozzer A (2015) The contribution of outdoor air pollution sources to premature mortality on a global scale. *Nature* 525(7569):367–371. <https://doi.org/10.1038/nature15371>
- Kennepohl D, Farmer S, Reuch W (2019) Libre Texts Chemistry, Chapter 11: infrared spectroscopy and mass spectrometry, infrared spectra of some common functional groups, virtual textbook of organic chemistry. [https://chem.libretexts.org/Bookshelves/Organic\\_Chemistry/Map%3A\\_Organic\\_Chemistry\\_\(Wade\)\\_Complete\\_and\\_Semesters\\_I\\_and\\_II/Map%3A\\_Organic\\_Chemistry\\_\(Wade\)/11%3A\\_Infrared\\_Spectroscopy\\_and\\_Mass\\_Spectrometry/11.05%3A\\_Infrared\\_Spectra\\_of\\_Some\\_Common\\_Functional\\_Groups](https://chem.libretexts.org/Bookshelves/Organic_Chemistry/Map%3A_Organic_Chemistry_(Wade)_Complete_and_Semesters_I_and_II/Map%3A_Organic_Chemistry_(Wade)/11%3A_Infrared_Spectroscopy_and_Mass_Spectrometry/11.05%3A_Infrared_Spectra_of_Some_Common_Functional_Groups). Accessed 15 Mar 2023
- Mandal P, Saud T, Sarkar R, Mandal A, Sharma SK, Mandal TK, Bassin JK (2014) High seasonal variation of atmospheric C and particulate concentrations in Delhi, India. *Environ Chem Lett* 12:225–230. <https://doi.org/10.1007/s10311-013-0438-y>
- Merck (2023) IR Spectrum Table & Chart. <https://www.sigmaaldrich.com/IN/en/technical-documents/technical-article/analytical-chemistry/photometry-and-reflectometry/ir-spectrum-table>. Accessed 15 Mar 2023
- Mohr C, Lopez-Hilfiker FD, Zotter P, Prévôt ASH, Xu L, Ng NL, Herndon SC, Williams LR, Franklin JP, Zahniser MS, Worsnop DR, Knighton WB, Aiken AC, Gorkowski KJ, Dubey MK, Allan JD, Thornton JA (2013) Contribution of nitrated phenols to wood burning brown carbon light absorption in detling, United Kingdom during winter time. *Environ Sci Technol* 47:6316–6324. <https://doi.org/10.1021/es400683v>
- Murari V, Kumar M, Singh N, Singh RS (2016) Particulate morphology and elemental characteristics: variability at middle Indo-Gangetic Plain. *J Atmos Chem* 73:165–179. <https://doi.org/10.1007/s10874-015-9321-5>
- Neupane BB, Sharma A, Giri B, Joshi MK (2020) Characterization of airborne dust samples collected from core areas of Kathmandu Valley. *Heliyon* 6(4). <https://doi.org/10.1016/j.heliyon.2020.e03791>
- Pachauri T, Singla V, Satsangi A, Lakhani A, Kumari KM (2013) SEM-EDX characterization of individual coarse particles in Agra, India. *Aerosol Air Qual Res* 13:523–536. <https://doi.org/10.4209/aaqr.2012.04.0095>
- Panwar P, Prabhu V, Soni A (2020) Sources and health risks of atmospheric particulate matter at Bhagwanpur, an industrial site along the Himalayan foothills. *SN Appl Sci* 2:632. <https://doi.org/10.1007/s42452-020-2420-1>
- Pongpiachan S, Thumanu K, Chantharakhon C, Phoomalee C, Tharasawatpipat C, Apiratikul R, Poshychinda S (2022) Applying synchrotron radiation-based attenuated total reflection-Fourier transform infrared to evaluate the effects of shipping emissions on fluctuations of PM<sub>10</sub>-bound organic functional groups and ionic species. *Atmos Pollut Res* 13(9):101517. <https://doi.org/10.1016/j.apr.2022.101517>
- Pope CA, Dockery DW (2006) Health effects of fine particulate air pollution: lines that connect. *JAPCA* 56:709–742. <https://doi.org/10.1080/10473289.2006.10464485>
- Pope CA, Ezziati M, Dockery DW (2009) Fine-particulate air pollution and life expectancy in the United States. *New Engl J Med* 360:376–386. <https://doi.org/10.1056/NEJMSa0805646>
- Rai A, Mukherjee S, Chatterjee A, Choudhary N, Kotnala G, Mandal TK, Sharma SK (2020) Seasonal variation of OC, EC, and WSOC of PM<sub>10</sub> and their CWT Analysis over the eastern Himalaya. *Aerosol Sci Eng* 4:26–40. <https://doi.org/10.1007/s41810-020-00053-7>



- Rai A, Mukherjee S, Choudhary N, Ghosh A, Chatterjee A, Mandal TK, Sharma SK, Kotnala R (2021) Seasonal transport pathway and sources of carbonaceous aerosols at an urban site of eastern Himalaya. *Aerosol Sci Eng* 5:318–343. <https://doi.org/10.1007/s41810-021-00106-5>
- Ram K, Sarin MM (2011) Day–night variability of EC, OC, WSOC and inorganic ions in urban environment of Indo–Gangetic Plain: implications to secondary aerosol formation. *Atmos Environ* 45:460–468. <https://doi.org/10.1016/j.atmosenv.2010.09.055>
- Ram K, Sarin MM (2012) Carbonaceous aerosols over Northern India: sources and spatio-temporal variability. *Proc Indian natn Sci Acad* 78(3):523–533
- Ram K, Sarin MM, Hegde P (2008) Atmospheric abundances of primary and secondary carbonaceous species at two high-altitude sites in India: sources and temporal variability. *Atmos Environ* 42:6785–6796. <https://doi.org/10.1016/j.atmosenv.2008.05.031>
- Ramanathan V, Crutzen PJ, Kiehl JT, Rosenfeld D (2001) Aerosols, climate, and the hydrological cycle. *Science* 294(5549):2119–2124. <https://doi.org/10.1126/science.1064034>
- Saraswati, Sharma SK, Saxena M, Mandal TK (2019) Characteristics of gaseous and particulate ammonia and their role in the formation of secondary inorganic particulate matter at Delhi, India. *Atmos Res* 218:34–49. <https://doi.org/10.1016/j.atmosres.2018.11.010>
- Sarkar C, Chatterjee A, Majumdar D, Ghosh SK, Srivastava A, Raha S (2014) Volatile organic compounds over Eastern Himalaya, India: temporal variation and source characterization using positive matrix factorization. *Atmos Chem Phys* 14(23):32133–32175. <https://doi.org/10.5194/acpd-14-32133-2014>
- Sarkar C, Chatterjee A, Majumdar D, Roy A, Srivastava A, Ghosh SK, Raha S (2017b) How the atmosphere over Eastern Himalaya, India is polluted with carbonyl compounds? Temporal variability and identification of sources. *Aerosol Air Qual Res* 17:2206–2223. <https://doi.org/10.4209/aaqr.2017.01.0048>
- Sarkar C, Sinha V, Sinha B, Panday AK, Rupakheti M, Lawrence MG (2017a) Source apportionment of NMVOCs in the Kathmandu Valley during the SusKat-ABC international field campaign using positive matrix factorization. *Atmos Chem Phys* 17:8129–8156. <https://doi.org/10.5194/acp-17-8129-2017>
- Seinfeld JH, Pandis SN (2016) *Atmospheric chemistry and physics: from air pollution to climate change*. Wiley, New York
- Shankar S, Gadi R, Bajar S, Yadav N, Mandal TK, Sharma SK (2023b) Insights into seasonal-variability of SVOCs, morpho-elemental and spectral characteristics of PM<sub>2.5</sub> collected at a dense industrial site: Faridabad, Haryana, India. *Chemosphere* 323:138204. <https://doi.org/10.1016/j.chemosphere.2023.138204>
- Shankar S, Gadi R, Sharma SK, Mandal TK (2022) Identification of carbonaceous species and FTIR profiling of PM<sub>2.5</sub> aerosols for source estimation in Old Delhi Region of India. *MAPAN* 37(3):529–544. <https://doi.org/10.1007/s12647-022-00575-0>
- Shankar S, Gadi R, Sharma SK, Mandal TK (2023a) Short-term effects: elemental and morphological assessment of aerosols over Old Delhi Region, India. *MAPAN*. <https://doi.org/10.1007/s12647-023-00646-w>
- Sharma SK, Choudhary N, Kotnala G, Das D, Mukherjee S, Ghosh A, Vijayan N, Rai A, Chatterjee A, Mandal TK (2020b) Wintertime carbonaceous species and trace metals in PM<sub>10</sub> in Darjeeling: a high altitude town in the eastern Himalayas. *Urban Clim* 34:100668. <https://doi.org/10.1016/j.uclim.2020.100668>
- Sharma SK, Choudhary N, Srivastava P, Naja M, Vijayan N, Kotnala G, Mandal TK (2020a) Variation of carbonaceous species and trace elements in PM<sub>10</sub> at a mountain site in the central Himalayan region of India. *J Atmos Chem* 77:1–14. <https://doi.org/10.1007/s10874-020-09402-9>
- Sharma SK, Mandal TK (2023) Elemental composition and sources of fine particulate matter (PM<sub>2.5</sub>) in Delhi, India. *Bull Environ Contam Toxicol* 110:60. <https://doi.org/10.1007/s00128-023-03707-7>
- Sharma SK, Mandal TK, Jain S, Saraswati, Sharma A, Saxena M (2016) Source apportionment of PM<sub>2.5</sub> in Delhi, India using PMF model. *Bull Environ Contam Toxicol* 97:286–293. <https://doi.org/10.1007/s00128-016-1836-1>
- Sharma SK, Mandal TK, Sharma C, Kuniyal JC, Joshi R, Dhyani PP, Rohtash, Ghayas H, Gupta NC, Sharma P, Saxena M, Sharma A, Arya BC, Kumar A (2014) Measurements of particulate (PM<sub>2.5</sub>), BC and trace gases over the Northwestern Himalayan region of India. *Mapan* 29(4):243–253. <http://npl.csircentral.net/id/eprint/1402>
- Sharma SK, Mukherjee S, Choudhary N, Rai A, Ghosh A, Chatterjee A, Vijayan N, Mandal TK (2021) Seasonal variation and sources of carbonaceous species and elements in PM<sub>2.5</sub> and PM<sub>10</sub> over the eastern Himalaya. *Environ Sci Pollut Res* 28:51642–51656. <https://doi.org/10.1007/s11356-021-14361-z>
- Shashni S, Kuniyal JC, Sharma G, Julka JM (2018) Particulate (PM<sub>10</sub>) and gaseous pollutants (NO<sub>2</sub>, SO<sub>2</sub>) and their sources in the Tirthan valley of the great Himalayan National Park, North-Western Himalaya, India. *Int J Adv Res* 6(12):1253–1262. <https://doi.org/10.21474/IJAR01/8261>
- Sheoran R, Dumka UC, Kaskaoutis DG, Grivas G, Ram K, Prakash J, Hooda RK, Tiwari RK, Mihalopoulos N (2021) Chemical composition and source apportionment of total suspended particulate in the central Himalayan region. *Atmosphere* 12:1128. <https://doi.org/10.3390/atmos12091228>
- Shivani, Gadi R, Sharma SK, Mandal TK (2019) Seasonal variation, source apportionment and source attributed health risk of fine carbonaceous aerosols over National Capital Region, India. *Chemosphere* 237:124500. <https://doi.org/10.1016/j.chemosphere.2019.124500>
- Singh RK (2019) Assessment of ambient air pollution and mitigation strategies towards Achieving Air Quality Index (AQI) in the Indian Himalayan Region. *Int J Sci Res* 9(12). <https://doi.org/10.21275/SR201228065047>
- Song Y, Zhang Y, Xie S, Zeng L, Zheng M, Salmon L, Shao M, Slanina S (2006) Source apportionment of PM<sub>2.5</sub> in Beijing by positive matrix factorization. *Atmos Environ* 40:1526–1537. <https://doi.org/10.1016/j.atmosenv.2005.10.039>
- Sreejith MV, Thomas JR, Aravindakumar CT, Aravind UK (2020) Characterisation of atmospheric particulate matter over a site in southern Kerala, India - using ATR-FTIR and confocal micro-Raman spectroscopy. *Mater Today: Proc* 33(2):1410–1414. <https://doi.org/10.1016/j.matpr.2020.05.783>
- Stuart BH (2004) *Infrared spectroscopy: fundamental and applications*. John Wiley and Sons
- Uria-Tellaetxe I, Carslaw DC (2014) Conditional bivariate probability function for source identification. *Environ Model Softw* 59:1–9. <https://doi.org/10.1016/j.envsoft.2014.05.002>
- Yao L, Fan X, Yan C, Kurtén T, Daellenbach KR, Li C, Wang Y, Guo Y, Dada L, Rissanen MP, Cai J, Tham YJ, Zha Q, Zhang S, Du W, Yu M, Zheng F, Zhou Y, Kontkanen J et al (2020) Unprecedented ambient sulfur trioxide (SO<sub>3</sub>) detection: possible formation mechanism and atmospheric implications. *Environ Sci Technol Lett* 7(11):809–818. <https://doi.org/10.1021/acs.estlett.0c00615> <https://himachaltourism.gov.in/wp-content/uploads/2023/03/Tourist-Statistics.pdf>

**Publisher's Note** Springer Nature remains neutral with regard to jurisdictional claims in published maps and institutional affiliations.

Springer Nature or its licensor (e.g. a society or other partner) holds exclusive rights to this article under a publishing agreement with the author(s) or other rightsholder(s); author self-archiving of the accepted manuscript version of this article is solely governed by the terms of such publishing agreement and applicable law.